n-Alkane Characteristics of Thawed Permafrost Deposits Below a Thermokarst Lake on Bykovsky Peninsula, Northeastern Siberia

Loeka L. Jongejans[1,2]*, Kai Mangelsdorf[3], Lutz Schirrmeister[1], Mikhail N. Grigoriev[4], Georgii M. Maksimov[4], Boris K. Biskaborn[5], Guido Grosse[1,2] and Jens Strauss[1]

[1] Section of Permafrost Research, Alfred Wegener Institute, Helmholtz Centre for Polar and Marine Research, Potsdam, Germany, [2] Institute of Geosciences, University of Potsdam, Potsdam, Germany, [3] Section of Organic Geochemistry, GFZ German Research Centre for Geosciences, Potsdam, Germany, [4] Laboratory of General Geocryology, Melnikov Permafrost Institute, Siberian Branch of the Russian Academy of Sciences, Yakutsk, Russia, [5] Section of Polar Terrestrial Environmental Systems, Alfred Wegener Institute Helmholtz Centre for Polar and Marine Research, Potsdam, Germany

Rapid permafrost thaw by thermokarst mobilizes previously frozen organic matter (OM) down to tens of meters deep within decades to centuries, leading to microbial degradation and greenhouse gas release. Late Pleistocene ice-rich Yedoma deposits that thaw underneath thermokarst lakes and refreeze after lake drainage are called taberal sediments. Although widespread, these have not been the subject of many studies. To study OM characteristics and degradability in thawed Yedoma, we obtained a 31.5 m long core from beneath a thermokarst lake on the Bykovsky Peninsula, northeastern Siberia. We reported radiocarbon ages, biogeochemical parameters [organic carbon (OC) content and bulk carbon isotopes] and *n*-alkane distributions. We found the most degraded OM in frozen, fluvial sediments at the bottom of the core, as indicated by the lowest *n*-alkane odd-over-even predominance (OEP; 2.2). Above this, the thawed Yedoma sediments had an *n*-alkane distribution typical of emergent vegetation, suggesting a landscape dominated by low-centered polygons. These sediments were OC poor (OC content: 0.8 wt%, 60% of samples < 0.1 wt%), but the OM (OEP~5.0) was better preserved than in the fluvial sediments. The upper part of the Yedoma reflected a transition to a drier, grass dominated environment. Furthermore, this unit's OM was least degraded (OEP~9.4). The thermokarst lake that formed about 8 cal ka BP thawed the Yedoma in the talik and deposited Holocene lake sediments containing well-preserved OM (OEP~8.4) with the highest *n*-alkane concentrations (20.8 μg g^{-1} sediment). Old, allochthonous OM was found in the thawed Yedoma and frozen fluvial deposits. Using an *n*-alkane endmember model, we identified a mixed OM input in all units. In our study, the thawed Yedoma sediments contained less OC than reported in other studies for still frozen Yedoma. The Yedoma OM was more degraded compared to previous biomarker research on frozen Yedoma. However, this signal is

overprinted by the input signal. The fluvial deposits below the Yedoma contained more OM, but this OM was more degraded, which can be explained by the OM input signal. Continued talik deepening and expansion of this thermokarst lake and others similar to it will expose OM with heterogeneous properties to microbial degradation.

INTRODUCTION

Current climate change is causing rapid changes in the Arctic. Accordingly, permafrost deposits are warming and thawing in many regions including Siberia (Biskaborn et al., 2019). Thawing leads to increased microbial decomposition of the previously freeze-locked organic matter (OM) (Mackelprang et al., 2011; Schuur et al., 2015). The amount of organic carbon (OC) that may be mobilized from thawed permafrost sediments is constrained by the OM quantity and quality. Top-down thaw by deepening of the seasonally thawed layer (active layer) largely affects OM in the active layer and near surface permafrost, some of which has already been influenced by early Holocene deeper active layer thaw (French, 1999; Lacelle et al., 2019). Deep permafrost thaw processes, however, such as thermokarst development, may expose OM from Late Pleistocene permafrost deposits to microbial degradation down to tens of meters deep for the first time (Heslop et al., 2019; Turetsky et al., 2020).

Ice-rich, syngenetic Yedoma deposits are late Pleistocene permafrost deposits that are widespread in northern Siberia and Alaska (Schirrmeister et al., 2013) and contain a significant OC pool (Strauss et al., 2013; Hugelius et al., 2014). Yedoma deposits that thaw *in situ* in taliks underneath thermokarst lakes become diagenetically altered due to ice-loss and compaction. Following lake drainage, these talik sediments can refreeze again, after which they are called taberal sediments: *in situ* thawed, diagenetically altered and refrozen sediments (Romanovskii, 1993). Strauss et al. (2013) estimated that about 10% of the Yedoma region is covered by lakes and rivers and 56% by drained lake basins with likely refrozen taberal deposits. After thawing of the Yedoma deposits, anaerobic conditions in the water-logged compacted talik sediments promote methane production (Zimov et al., 1997; Walter et al., 2006). Although spatially widespread, taberal sediments have not been subject of many studies yet and are rarely included in OC storage estimates or studies of OM degradability.

A first estimate of the taberal deposit OC pools suggests ∼114 Gt OC, which is about 25% of the Yedoma domain OC storage (∼398 Gt) (Walter Anthony et al., 2014; Strauss et al., 2017). In several studies, it is also shown that the OM degradability in Yedoma deposits is higher compared to that in Holocene deposits (Knoblauch et al., 2013; Strauss et al., 2015; Jongejans et al., 2018; Stapel et al., 2018). However, the fate of OM in Yedoma deposits affected by thawing and subsequent qualitative and quantitative changes is poorly understood. Various studies indicate that OM from thawed Yedoma becomes partially degraded. For example, Wetterich et al. (2009) found
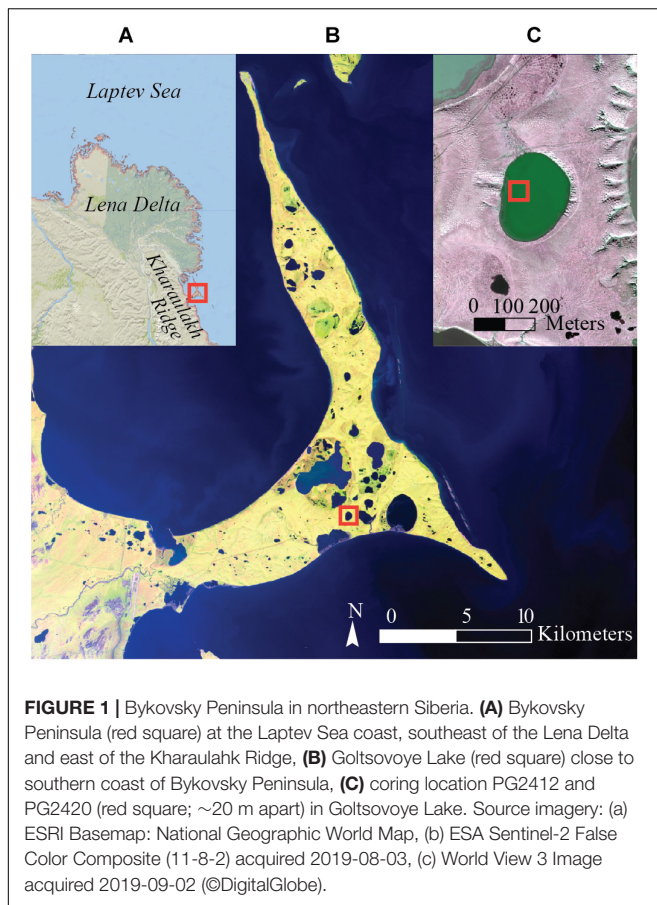
that plant material was further degraded in taberal deposits than in Yedoma deposits in the Dmitry Laptev Strait.

The study of the biomolecules and other OM characteristics can give important insights into OM degradability and could hence greatly improve estimates of permafrost OM mobilization (Andersson and Meyers, 2012; Sánchez-García et al., 2014). A few studies have previously focused on molecular biomarkers in northeastern Siberian permafrost deposits (Zech et al., 2010; Höfle et al., 2013; Strauss et al., 2015; Stapel et al., 2018). In general, the abundance and distribution of *n*-alkanes, which are long-chained, single bonded hydrocarbons, are used as indicator for OM characterization. The length of *n*-alkanes is an indicator for OM source. Long chained *n*-alkanes (>22 carbon atoms) mainly originate from vascular plants, for example in leaf waxes, whereas short chains (12–20 carbon atoms) are produced by bacteria and algae (Killops and Killops, 2013). The ratio of odd to even chains – expressed as carbon preference index (CPI) (Bray and Evans, 1961; Marzi et al., 1993) or odd-over-even predominance (OEP) (Zech et al., 2009; Struck et al., 2019) – is an indicator for OM degradability and decreases with ongoing alteration of the OM. Furthermore, several studies in temperate latitudes showed that relative *n*-alkane proportions can be used to distinguish between vegetation types. n-C_{23} and n-C_{25} are predominant in aquatic macrophytes and *Sphagnum* mosses (Ficken et al., 1998; Bingham et al., 2010; Bush and McInerney, 2013), n-C_{27} and n-C_{29} are mainly produced by trees and shrubs, and n-C_{31} and n-C_{33} mostly derive from grasses and herbs (Zech et al., 2009; Schäfer et al., 2016). Very few comparable studies were carried out for talik or taberal sediments (Romankevich et al., 2017; Ulyantsev et al., 2017).

Thus, for the first time we present molecular biomarker characteristics from Yedoma deposits thawed *in situ* in the talik underneath a thermokarst lake. This study aims to answer the following research questions: (1) what is the sedimentation history of the Yedoma deposits at the study site and (2) what is the OM degradation potential of Yedoma deposits already thawed in a talik?

STUDY AREA

To answer these research questions, we analyzed a 31.5 m long sediment core from sediments underneath Goltsovoye Lake, a thermokarst lake on Bykovsky Peninsula in northeastern Siberia. The Bykovsky Peninsula is a remnant of a former late Pleistocene Yedoma accumulation plane, situated in the foreland of the Kharaulakh Ridge at the Laptev Sea coast (**Figure 1**).

FIGURE 1 | Bykovsky Peninsula in northeastern Siberia. **(A)** Bykovsky Peninsula (red square) at the Laptev Sea coast, southeast of the Lena Delta and east of the Kharaulahk Ridge, **(B)** Goltsovoye Lake (red square) close to southern coast of Bykovsky Peninsula, **(C)** coring location PG2412 and PG2420 (red square; ∼20 m apart) in Goltsovoye Lake. Source imagery: (a) ESRI Basemap: National Geographic World Map, (b) ESA Sentinel-2 False Color Composite (11-8-2) acquired 2019-08-03, (c) World View 3 Image acquired 2019-09-02 (©DigitalGlobe).

The area is characterized by continuous permafrost, which reaches depths down to 600 m (Grigoriev, 1960). The modern surface morphology is characterized mainly by Yedoma uplands (up to 45 m a.s.l.) and thermokarst depressions and lakes, as well as thermal erosional valleys (Siegert et al., 2002; Grosse et al., 2007). Nival and slope processes in the nearby Kharaulakh Ridge and *in situ* frost weathering after deposition led to the formation of the Yedoma uplands in the mountain foreland during the late Pleistocene (Schirrmeister et al., 2002a; Strauss et al., 2012). Strong permafrost degradation since the late Pleistocene to early Holocene transition resulted in thermokarst development and thermal erosion of the Yedoma uplands, which characterize the modern relief of the Bykovsky Peninsula (Grosse et al., 2005). The Bykovsky Peninsula is covered by about 14.4% by thermokarst lakes and lagoons while 46.1% are covered by drained thermokarst lake basins (Grosse et al., 2005).

Goltsovoye Lake (71.74515°N, 129.30217°E) is a medium-sized thermokarst lake (dimensions: 630 by 480 m, surface: ∼23 ha) located close to the southern coast of the peninsula (**Figure 1**). The lake reaches a water depth of about 5 m and has a talik reaching about 30 m deep (Strauss et al., 2018). It is mainly surrounded by Yedoma deposits that are eroded along the lake shore, and drained thermokarst lake basins which are characterized by ice wedge polygons. Several other thermokarst lakes in the vicinity transitioned to thermokarst

lagoons already due to coastal erosion and inundation with sea water, allowing salt water to interact with the former freshwater taliks (Jenrich, 2020).

Previous permafrost research on the Bykovsky Peninsula included cryostratigraphical and cryolithological research on Yedoma and thermokarst-affected deposits (Kunitsky, 1989; Slagoda, 1993; Schirrmeister et al., 2002a,b, 2018; Slagoda, 2004, 2005; Grosse et al., 2007; Romankevich et al., 2017; Ulyantsev et al., 2017). The total organic carbon (TOC) content of Yedoma deposits on the east coast of the Bykovsky Peninsula (Mamontovy Khayata) ranges from 2 to 14 wt%, whereas Holocene cover deposits on top of the Yedoma have a TOC between 2 and 27 wt% (Schirrmeister et al., 2002a). In a transect study in the central part of Bykovsky Peninsula, Fuchs et al. (2018) found mean TOC values of 5.1 ± 4.3 wt% for the upper 3 m on Yedoma uplands consisting of Holocene cover deposits and 7.9 ± 9.0 wt% for drained thermokarst lake basin deposits.
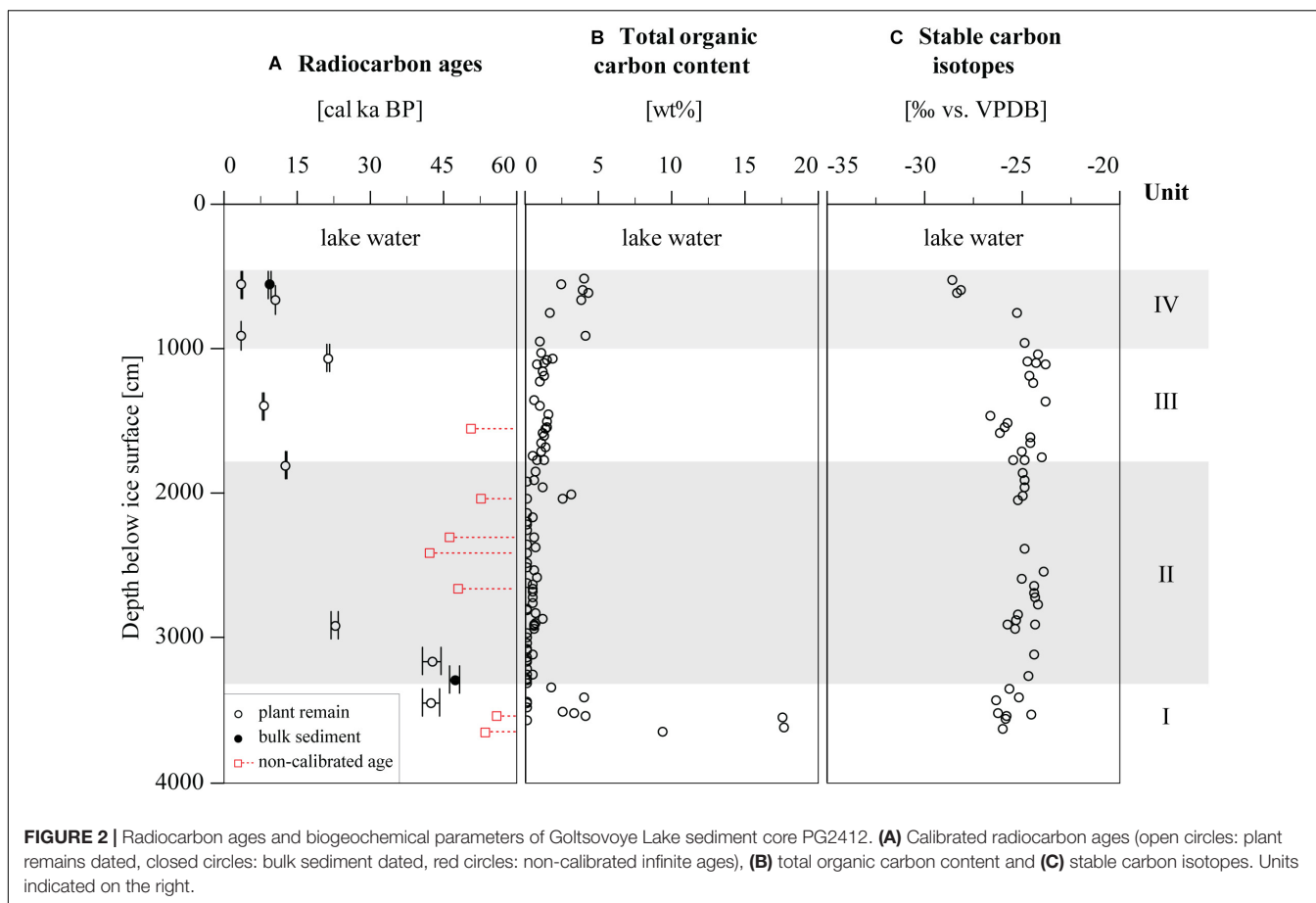
Despite the coastal setting, the modern climate of the Bykovsky Peninsula is rather continental with long, severe winters (September-May) and short, cold summers. The mean air temperature (2000–2016) is −29°C in January and +8°C in July (Tiksi Hydrometeorological Observatory) and the mean annual precipitation is less than 350 mm. Mean ground temperatures reach −9 to −11°C. This region is dominated by moss-grass low shrub tundra and is therefore classified as northern tundra (Treshnikov, 1985).

MATERIALS AND METHODS

Field Work

Field work on the Bykovsky Peninsula was carried out in April 2017 (Strauss et al., 2018). Over the course of 4 days, a 31.5-m long sediment core (PG2412; 71.74515°N, 129.30217°E) was retrieved from the deepest point in Goltsovoye Lake (**Figure 1**), using a URB2-4T drilling rig placed on a truck. The ice cover of the thermokarst lake was 195 cm thick and sediments started at 510 cm from the ice surface. For the depth assignment of the sample material, the water column with the ice cover was included (e.g., see **Figure 2**). Thus, depth measurements started at the ice surface. The core consisted of unfrozen talik sediments (until 3425 cm) and frozen sediments below the talik. The upper few meters of sediment consist of gray silty, fine sand and include plant remains and biogenic shells. Deeper in the core, coarser sandy intervals containing 2-cm-big pebbles alternate with fine sand intervals with large wooden remains. In general, abundant wooden remains and organic-enriched layers were observed between 3665 and 1900 cm. The core material was documented and protected and transported frozen to Potsdam for subsampling. During drilling, core loss happened in the intervals: 3550–3510 cm, 2135–2050 cm and 910–755 cm.

We compare the data from the PG2412 sediment core with the data from a 5 m long sediment core (PG2420; 71.74530°N, 129.30243°E) that was drilled ∼20 m away from PG2412, using a UWITEC piston coring system (Strauss et al., 2018; Biskaborn and Sens, 2020). From here on, we will refer to core PG2412 as the long core and PG2420 as the short core.

FIGURE 2 | Radiocarbon ages and biogeochemical parameters of Goltsovoye Lake sediment core PG2412. **(A)** Calibrated radiocarbon ages (open circles: plant remains dated, closed circles: bulk sediment dated, red circles: non-calibrated infinite ages), **(B)** total organic carbon content and **(C)** stable carbon isotopes. Units indicated on the right.

Laboratory Analyses

The long core was described in detail and subsampled for laboratory analyses. Pore water was extracted from thawed samples using rhizon soil moisture samples (membrane pore size: 0.12–0.18 μm). The pH and electrical conductivity (μS cm^{-1}) were measured from the pore water. The sediment samples were freeze-dried and the water content was determined based on the weight difference before and after drying.

Eighteen samples were selected for radiocarbon dating from the long core. Macrofossils such as plant (sedges and twigs) and wooden remains were dated using Accelerator Mass Spectrometry in the AWI MICADAS Laboratory in Bremerhaven. For two of the samples, bulk sediment was dated due to the lack of visible macrofossils. Radiocarbon dates were calibrated using the CALIB 7.1 software and the IntCal13 calibration curve, and expressed as calibrated kilo years before present (cal ka BP) (Stuiver et al., 2017).

The grain size distribution of 71 samples from the long core was measured with a laser particle size analyzer (Malvern Mastersizer 3000, <1 mm fraction) after removal of organic material by treating the samples with hydrogen peroxide (30%). The samples were washed, freeze-dried, manually homogenized and sieved (<1 mm fraction measured) before measuring. Here, we show the grain size distribution of the fraction from 0.1 μm to 1 mm.

Homogenized bulk samples (n = 92, sample interval: ~35 cm) from the long core were analyzed for total nitrogen (TN) and total carbon (TC; Elementar Vario El III), and total organic carbon (TOC; Elementar Vario Max C), which are expressed in weight percentage (wt%). The stable carbon isotopic composition was determined for all samples with TOC values above the detection limit (0.1 wt%). The measured δ^{13}C (Thermo Fisher Scientific Delta-V-Advantage gas mass spectrometer equipped with a FLASH elemental analyzer EA 2000 and a CONFLO IV gas mixing system) is compared to the standardized Vienna Pee Dee Belemnite (VPDB) and expressed in per mille (‰ vs. VPDB). TOC values below the detection limit were not considered in further calculations.

For the short core, the same methods were used for radiocarbon dating, TOC content and stable carbon isotopes.

Biomarker Analysis

Twenty three samples from the long core were analyzed for lipid biomarkers at the German Research Centre for Geosciences (GFZ) after Schulte et al. (2000). Extraction of OM was done with a Dionex 200 ASE extractor using dichloromethane/methanol (DCM/MeOH, 99:1 v/v, heating phase 5 min, static phase 20 min at 75°C and 5 MPa). The extracts were passed over a sodium sulfate column with *n*-hexane and four internal standards were added for compound quantification: 5α-androstane, ethylpyrene,

5α-androstan-17-one and erucic acid. Using medium-pressure liquid chromatography (MPLC) after Radke et al. (1980), the extracts were separated into an aliphatic, aromatic and NSO (nitrogen-, sulfur- and oxygen-containing compounds) fraction.

n-Alkanes were measured in the aliphatic fraction using gas chromatography/mass spectrometry (GC-MS; GC Trace GC Ultra and MS DSQ, Thermo Electron Corporation) as described by Jongejans et al. (2018) (capillary column from BPX5, 22 mm × 50 m, 0.25 μm). Compounds were identified and quantified with respect to the internal standards from full scan mass spectra (m/z 50–600 Da, 2.5 scans s^{-1}) using the software XCalibur.

Biomarker Indices

The total lipid concentration of n-alkanes is expressed in microgram per gram of sediment (μg g^{-1} sed.) and per gram of TOC (μg g^{-1} TOC).

The average chain length (ACL) of n-alkanes provides a measure for the main focus of the n-alkane chain length distribution and is used to identify OM source. Long-chain n-alkanes are produced by terrestrial higher plants for instance in mosses (n-C$_{23}$ and n-C$_{25}$), in leaf waxes (n-C$_{27}$ and n-C$_{29}$) and in grasses (n-C$_{31}$ and n-C$_{33}$) (e.g., 1998; Zech et al., 2009), whereas short-chain n-alkanes are mainly produced by bacteria and algae (Killops and Killops, 2013). The ACL was calculated for n-alkanes with carbon number 23–33 according to Equation (1) where i is the carbon number (Poynter and Eglinton, 1990).

$$ACL_{23-33} = \frac{\sum i \cdot C_i}{\sum C_i} \qquad (1)$$

The CPI and odd-over-even predominance (OEP) indicate the maturity of the OM. High values typically correspond to fresh, undegraded OM, and the ratios decrease with degradation (Bray and Evans, 1961; Marzi et al., 1993). The starting values depend on the composition of the source material. These indices were calculated following Equation (2) (Marzi et al., 1993) and (3) (Zech et al., 2009; Struck et al., 2019), respectively. As both indices are used in other studies, both parameters are presented here.

$$CPI_{23-33} = \frac{\sum odd\ C_{23-31} + \sum odd\ C_{25-33}}{2 \cdot \sum even\ C_{24-32}} \qquad (2)$$

$$OEP_{26-33} = \frac{\sum odd\ C_{27-33}}{\sum even\ C_{26-32}} \qquad (3)$$

Schäfer et al. (2016) developed an n-alkane endmember model to distinguish between trees and shrubs, and grasses and herbs. It is based on the n-alkane ratio (after Equation 4) and the OEP.

$$n - \text{Alkane ratio} = \frac{C_{31} + C_{33}}{C_{27} + C_{31} + C_{33}} \qquad (4)$$

In their pilot study, Ficken et al. (2000) proposed the proxy P$_{aq}$ for submerged or floating macrophytes (P$_{aq}$ > 0.4) versus emergent (0.1 < P$_{aq}$ < 0.4) and terrestrial plant input (P$_{aq}$ < 0.1; Equation 5).

$$P_{aq} = \frac{C_{23} + C_{25}}{C_{23} + C_{25} + C_{29} + C_{31}} \qquad (5)$$

As this proxy has only been used in tropical and temporal regions, we focus on the trend of the P$_{aq}$ and do not put weight on the proposed ranges. Zheng et al. (2007) developed the proxy P$_{wax}$ to express the share of OM derived from terrestrial plants (Equation 6).

$$P_{wax} = \frac{C_{27} + C_{29} + C_{31}}{\sum odd\ C_{23-31}} \qquad (6)$$

RESULTS

Based on clustering of the n-alkane parameters (see "n-Alkane Distributions"), we divided the long core into four units. Unit I ranged from 3665 to 3300 cm, Unit II from 3300 to 1800 cm, Unit III from 1800 to 1000 cm and Unit IV from 1000 to 510 cm. We decided to separate the results and discussion following the statistical clustering of the n-alkane parameters. The short core was divided into 3 units from the bottom to the top: Unit A from 1010 to 855 cm, Unit B1 from 855 to 820 cm and Unit B2 from 820 to 510 cm (**Figure 3**).
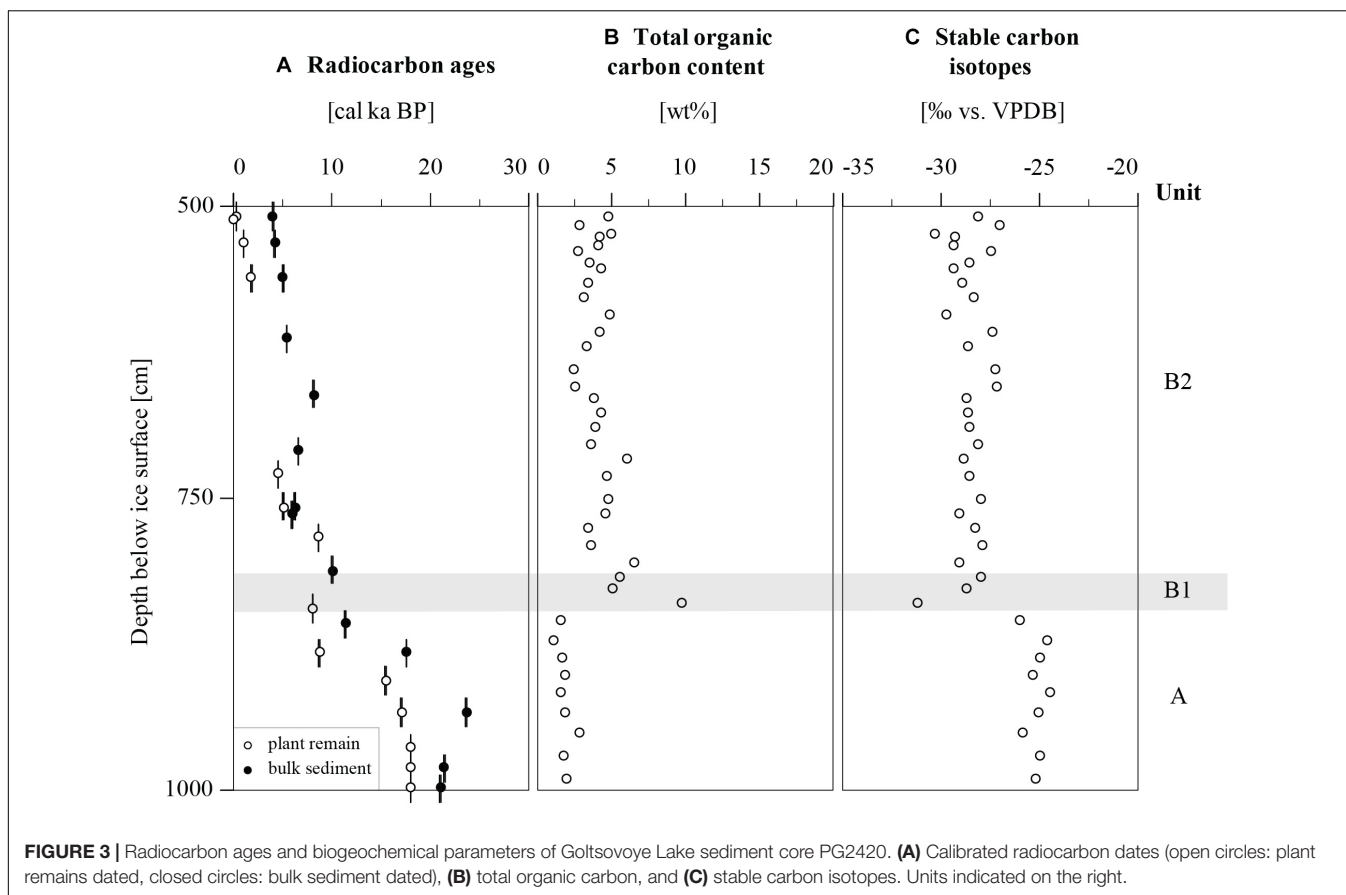
For both the long and the short core, we describe the radiocarbon ages and biogeochemical parameters (see section "Bulk Sediment"; **Figures 2**, **3**). For the long core, the hydrochemical parameters are characterized (see section "Hydrochemistry"; **Figure 4**), as well as the n-alkane parameters (see section "n-Alkane Distributions"; **Figure 5**). We further calculated general statistics for all parameters (**Supplementary Table 1**). All reported datasets were published in the open access PANGAEA archive (Biskaborn and Sens, 2020; Jongejans et al., 2020).

Bulk Sediment
Long Core PG2412

The calibrated radiocarbon ages of the macrofossils and bulk sediment of the long core (**Figure 2A**) showed a general trend over depth ranging from 47.5 cal ka BP at 3300 cm to 3.6 cal ka BP at 558 cm (surface sediments) (**Supplementary Table 2**). In Unit I, II and III, seven samples had an infinite age (i.e., below the radiocarbon detection limit; >42.4 to >56.1 ka BP) that could not be calibrated. Unit IV is of Holocene age. The bulk sediment at 558 cm was 5.7 ka older (9.3 cal ka BP) than the macro remains dated from the same sample (3.6 cal ka BP).

In the bottom of the core, the sediments were coarser (**Supplementary Figure 1**). Unit I contained coarse sand and rounded pebbles (up to 2 cm diameter), as well as finer sandy horizons that were mostly layered. The grain size distribution of Unit I and II (up to ~25 m) was predominantly unimodal indicating fine sand (**Supplementary Figure 1**). Units III and IV had a polymodal grain size distribution and the sediments were mostly very coarse silt to very fine sand.

During the drilling, the talik boundary was located at 3425 cm. Initial temperature data of the borehole (date: 2017-04-23), however, indicated the talik to be ~32 m deep (Strauss et al., 2018). Unit II, III, and IV were completely unfrozen. The cryostructure below 3425 cm was dominantly pore ice (ice between the organic remains) and partly structureless. Segregated ice was rare (ice lens at 3550 cm, 4 × 0.2 cm; ice band at 3592 cm, 1 cm thick).

FIGURE 3 | Radiocarbon ages and biogeochemical parameters of Goltsovoye Lake sediment core PG2420. **(A)** Calibrated radiocarbon dates (open circles: plant remains dated, closed circles: bulk sediment dated), **(B)** total organic carbon, and **(C)** stable carbon isotopes. Units indicated on the right.

Unit I was especially enriched in OM. Layers up to 30 cm thick containing twigs, stems, organic layers and lenses, and wooden remains up to 4 cm long in a frozen sandy matrix were found in the interval from 3665 to 3395 cm depth (**Supplementary Figure 2A**). Signs of cryoturbation were present at 3558 to 3555 cm (**Supplementary Figure 2B**). In the lowermost layer (3665-3650 cm), vertically oriented twigs up to 2 cm in length were discovered. Furthermore, organic remains were found from 2173–2311 cm, 1989–2050 cm, 1430–1590 cm, 950–1100, and 510–755 cm. The TOC was highest in the bottom of the core (maximum of 17.8 wt% at 3635 cm) (**Figure 2B**). Unit II and III were very OC poor, but TOC increased again in Unit IV (median: 1.1 wt%). The $\delta^{13}C$ ranged from −28.6‰ vs. VPDB in Unit IV (523 cm) to −23.8‰ vs. VPDB in Unit III (1370 cm) (median: −24.9‰ vs. VPDB).

Short Core PG2420

The short core was dated from 23.8 to 0 cal ka BP (**Figure 3A**) (Biskaborn and Sens, 2020). Unit A was deposited during the late Pleistocene, whereas Unit B1 and B2 were of Holocene age. The radiocarbon ages of Unit A ranged from 23.77 ± 0.06 cal ka BP (bulk sediment at 937 cm) to 11.41 ± 1 cal ka BP (bulk sediment at 860 cm). In Unit B, the samples had radiocarbon ages between 10.10 ± 0.05 cal ka BP (at 815 cm) and recent (at 514 cm, surface sediment). Almost all radiocarbon ages from bulk sediments were older than the respective picked plant remains (except for the

sample at 767 cm), with a maximum difference of 8.9 cal ka at 885 cm. However, both profiles show a general depth-related trend to older ages with increasing depth.

The sediments ranged from silty sand in Unit A to clayey silt in Unit B2. Unit B1 was composed of a peat layer. The sediments in Unit A were coarser than in Unit B1 and B2 (Strauss et al., 2018).

The TOC was lowest in Unit A (1.1 wt% at 875 cm), had its maximum in Unit B1 (9.8 wt% at 900 cm), and decreased to ∼4 wt% in Unit B2 (median: 3.6 wt%; **Figure 3B**).

The bulk carbon isotope ratio was highest in Unit A (−24.4‰ vs. VPDB at 920 cm) and lowest at the bottom of in Unit B1 (−31.2‰ vs. VPDB at 842 cm). Above, in Unit B2, the bulk d^{13}C signal ranged between −30.3 and −27.0‰ vs. VPDB (median: −28.2‰ vs. VPDB; **Figure 3C**).

Hydrochemistry

The water content of the long core ranged from 10.5 to 65.4 wt% and was highest in Unit I (frozen part) and the upper three samples of Unit IV (sediment surface samples) (median: 17.1 wt%; **Figure 4A**). There was not much variation in Unit II and III. The pH slightly increased from 7.2 in Unit I to 8.7 in Unit II, was relatively constant in Units II and III, but was much lower in the topmost three samples with the minimum of 6.3 at 596 cm (median: 8.2; **Figure 4B**). The electrical conductivity increased from Unit I to Unit II and decreased to the top from Unit III and IV (median: 778 μS cm^{-1};

FIGURE 4 | Hydrochemical parameters of Goltsovoye Lake sediment core PG2412. **(A)** Water content, **(B)** pH, and **(C)** electrical conductivity. Units indicated on the right.
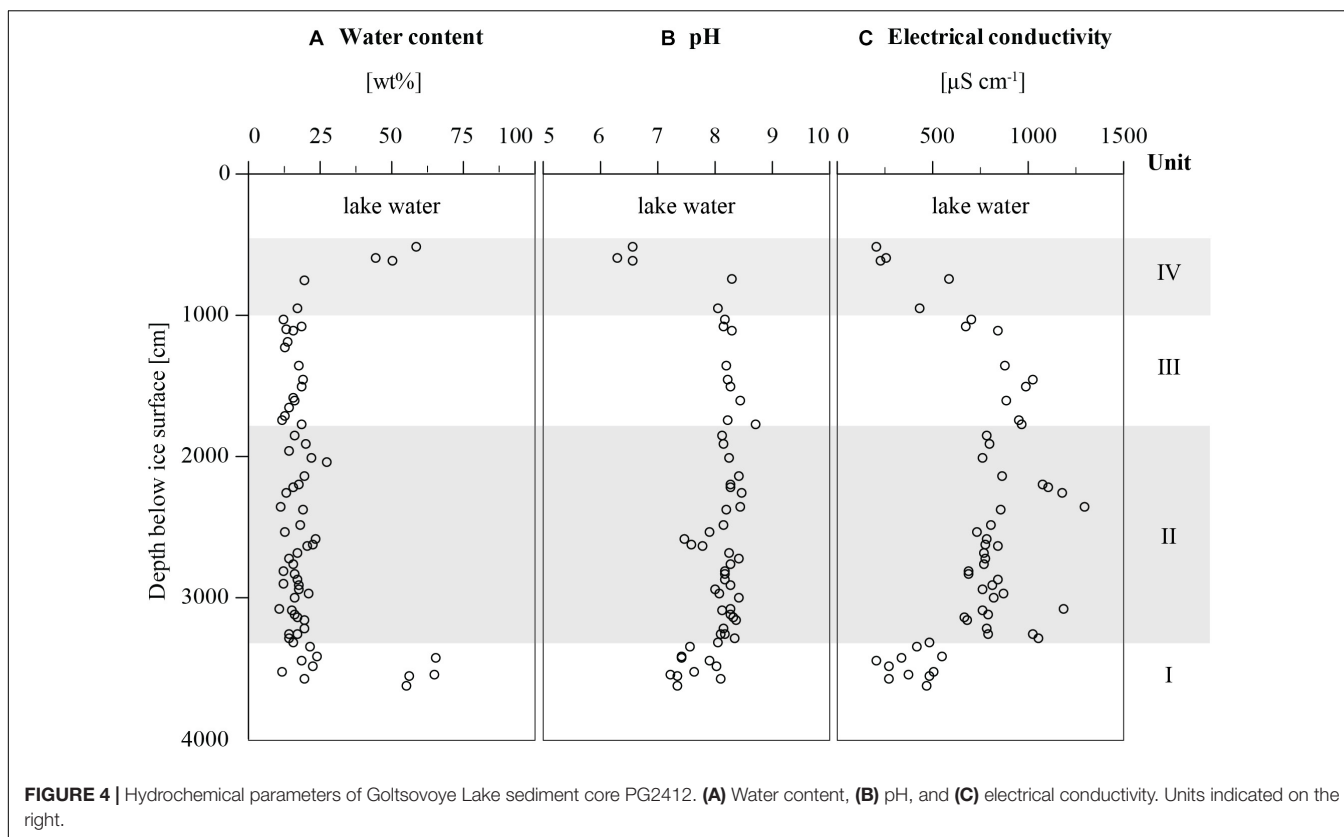
Figure 4C). In all hydrochemical parameters, the lowermost and uppermost samples of the core were substantially different from the middle part.

n-Alkane Distributions

The n-alkane concentration varied from 0.6 to 20.8 μg g^{-1} sed. (median: 1.8 μg g^{-1} sed.; **Figure 5A** and **Supplementary Table 3**). In contrast to the other samples of Unit I (median: 2.1 μg g^{-1} sed.), the lowermost sample showed a relatively high value (14.3 μg g^{-1} sed.). In Unit II and III, the n-alkane concentrations were generally low (median: 0.9 and 5.3 μg g^{-1} sed., respectively). In contrast, Unit IV was characterized by higher concentrations (median: 19.3 μg g^{-1} sed.). The n-alkane concentration per gram of TOC primarily increased from the bottom to the top of the core from 50.1 to 581.4 μg g^{-1} TOC with some stagnation in Unit II and III (median: 367.5 μg g^{-1} TOC; **Figure 5B** and **Supplementary Table 4**). The sediments were dominated by long-chain n-alkanes as indicated by a median ACL$_{23-33}$ of 27.5 (**Figure 5C**), representing the main focus of the n-alkane chain length distribution. The ACL increased from the bottom to the top and ranged from 26.5 in Unit I to 28.4 in Unit III. In Unit IV, the values were a bit lower again around 27.8. The CPI and OEP both increased stepwise from Unit I to II and III before they slightly decreased between Units III and IV. Overall, CPI and OEP were between 2.3 and 8.9 (median CPI: 4.8), and 2.2 and 11.0 (median OEP: 5.7), respectively (**Figure 5D**). The n-alkane

ratio ranged from 0.4 to 0.6 and was slightly higher in Units II and III (**Figure 5E**).

Clustering of the n-alkane data revealed four different units, which were also visible in the stepwise changes in the n-alkane proxies (**Figure 5**). These units seem to represent environmental changes reflected by different n-alkane distributions and were therefore used as subunits of the investigated sediment core (**Figure 5F**). All described n-alkane parameters were used as input for the clustering. Clustering was carried out in R v. 3.6.1 using the "chclust" function in package "rioja" with method "coniss."

Odd-carbon number chains dominated the n-alkane distributions of all samples. The dominating chain varied between mid- and long-chain n-alkanes (**Supplementary Figure 3**). Unit I was dominated by n-C$_{23}$ and n-C$_{25}$. Unit II and III were dominated by either n-C$_{27}$ or n-C$_{29}$. The upper samples from Unit III (1158 and 1070 cm) were dominated by n-C$_{31}$ and Unit IV again by n-C$_{27}$.

In order to see how the odd chains varied over depth with respect to each other, we calculated the relative n-alkane concentration per gram TOC for the odd chains C$_{23-33}$ (**Figure 6**). The n-C$_{33}$ was least abundant and showed a relatively constant depth profile. The n-C$_{27}$ and n-C$_{29}$ n-alkanes were most abundant. The relative concentration of n-C$_{23}$ and n-C$_{25}$ decreased upwards in the core, whereas n-C$_{31}$ generally increased upwards.

The P$_{aq}$ and P$_{wax}$ were strongly negatively correlated (Pearson correlation index $r = -0.995$, $p < 0.01$; **Figure 7**). The P$_{aq}$
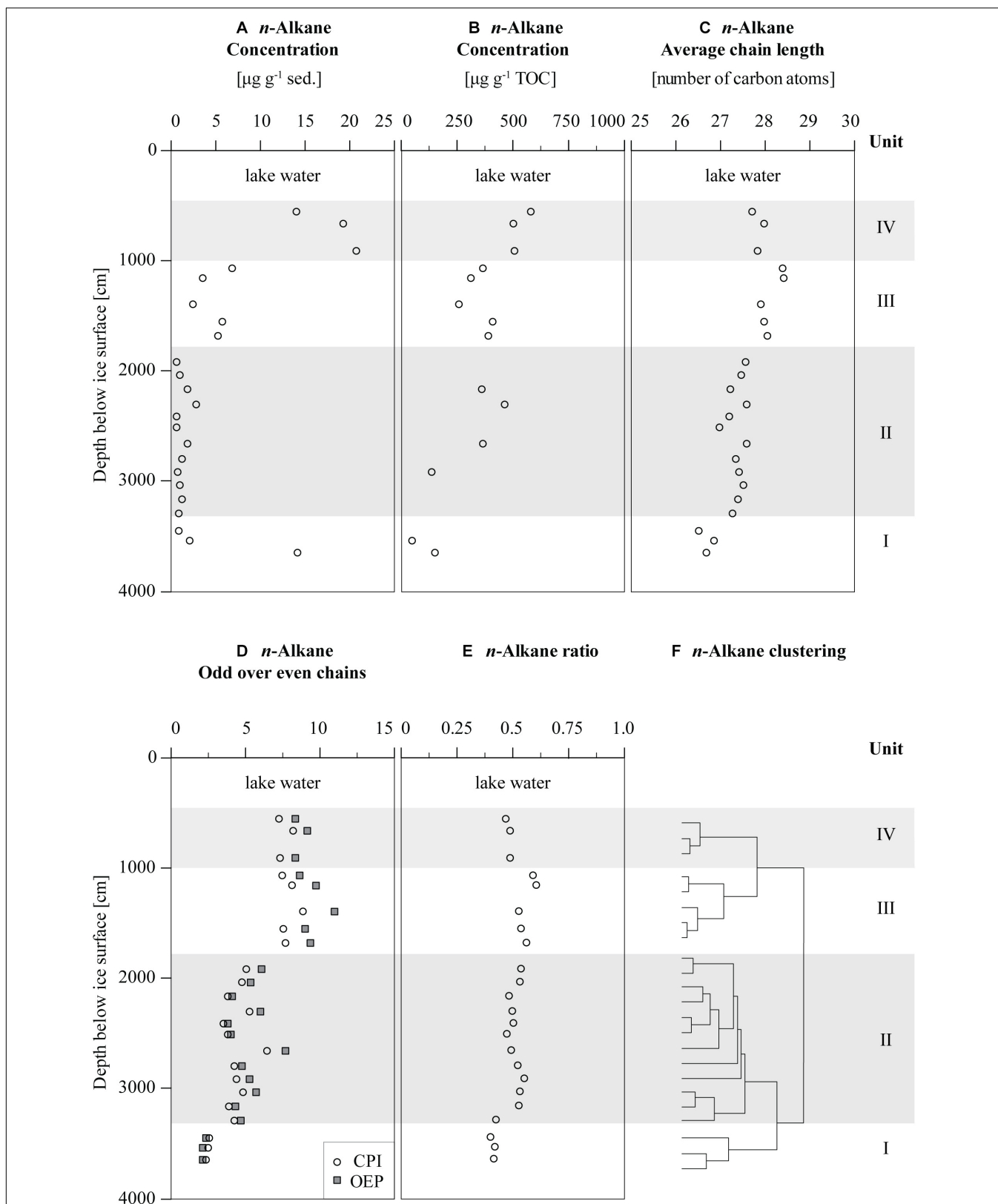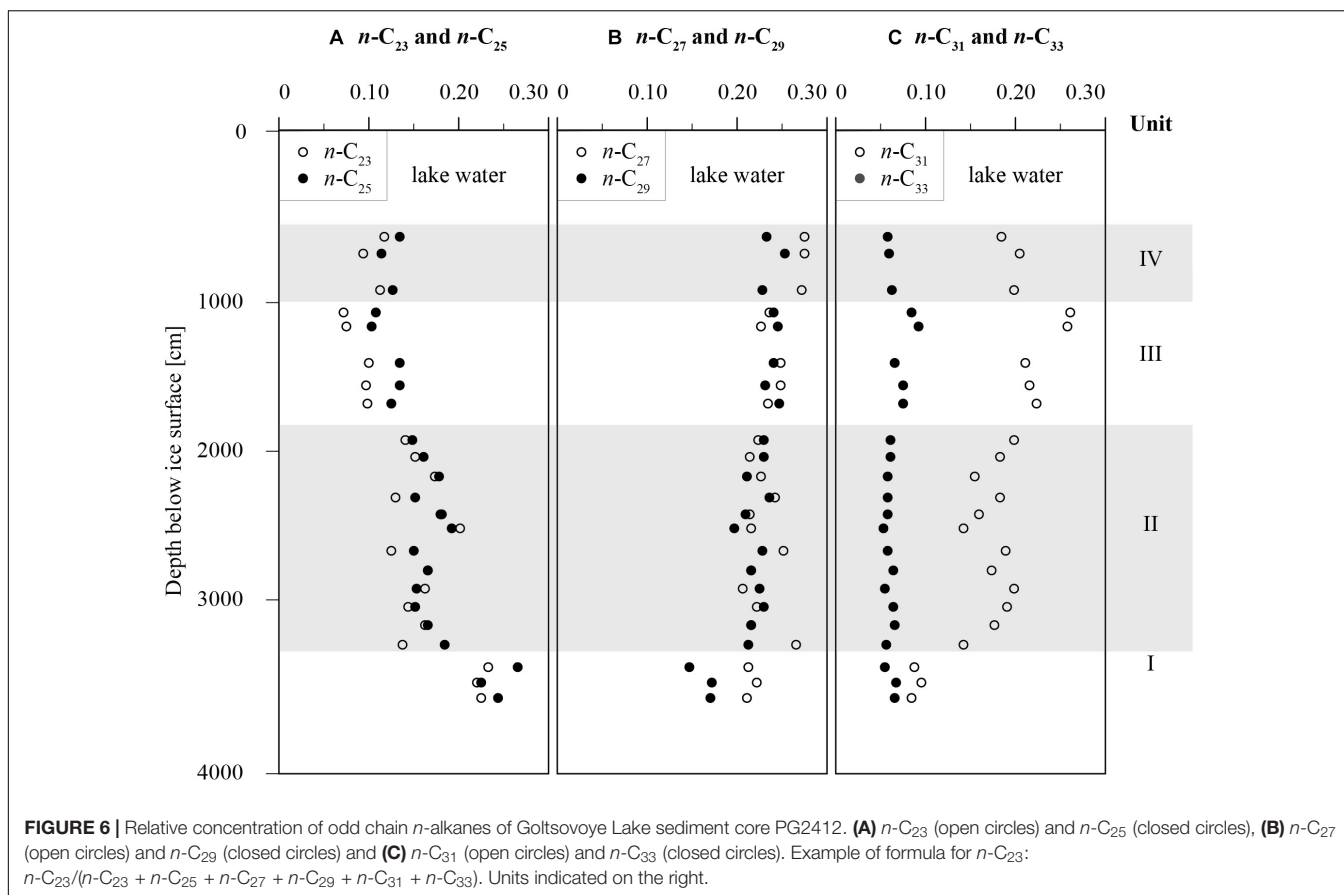
FIGURE 5 | *n*-Alkane parameters of Goltsovoye Lake sediment core PG2412. **(A)** *n*-Alkane concentration per gram sediment, **(B)** *n*-alkane concentration per gram organic carbon (note: samples with TOC < 0.1 wt% not shown), **(C)** *n*-alkane average chain length, **(D)** *n*-alkane carbon preference index (CPI) and odd-over-even predominance (OEP; gray squares), **(E)** *n*-alkane ratio (after Schäfer et al., 2016), and **(F)** *n*-alkane clustering. Units indicated on the right.

FIGURE 6 | Relative concentration of odd chain n-alkanes of Goltsovoye Lake sediment core PG2412. **(A)** $n\text{-}C_{23}$ (open circles) and $n\text{-}C_{25}$ (closed circles), **(B)** $n\text{-}C_{27}$ (open circles) and $n\text{-}C_{29}$ (closed circles) and **(C)** $n\text{-}C_{31}$ (open circles) and $n\text{-}C_{33}$ (closed circles). Example of formula for $n\text{-}C_{23}$: $n\text{-}C_{23}/(n\text{-}C_{23} + n\text{-}C_{25} + n\text{-}C_{27} + n\text{-}C_{29} + n\text{-}C_{31} + n\text{-}C_{33})$. Units indicated on the right.

decreased with depth with a maximum of 0.68 in Unit I and a minimum of 0.26 in Unit III (median: 0.41).

DISCUSSION

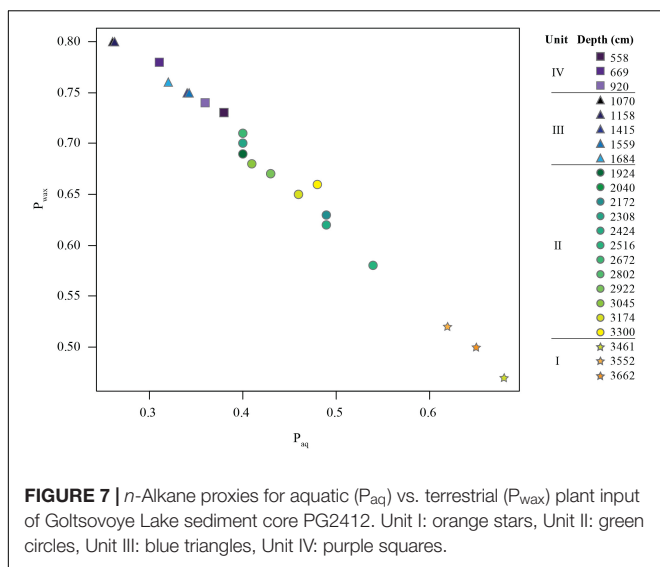### Depositional History at the Study Site

In the following, we discuss the sedimentation and post-depositional history of permafrost and lacustrine deposits on Bykovsky Peninsula based on sediment and biomarker parameters observed in our cores.

Generally, it should be noted that age reversals in the sediment core suggest that old organic material has been remobilized in the thermokarst lake environment, i.e., due to thaw and erosion of surrounding permafrost outcrops along the lake shore, which is typical for such dynamic environments (Lenz et al., 2016). Accordingly, the radiocarbon concentrations of bulk samples represent a mixture of reworked particulate organic matter and fresh organic material from the ecosystem at the time of deposition, causing bulk radiocarbon dates to be offset toward older ages compared to dated plant samples (see also Gaglioti et al., 2014).

The sedimentary record in our core starts with fluvial sediments that were deposited during the early Weichselian (see section "Unit I – Early Weichselian fluvial sedimentation"), after which Yedoma sedimentation took place (see sections

"Unit II – Yedoma Deposition in Wetland Landscapes Dominated by Low-Centered Polygons" and "Unit III/Unit A – Yedoma Deposition Under Cold-Dry Conditions During the Late Weichselian"). During the Holocene, a thermokarst lake formed, which thawed the Yedoma sediments and allowed the deposition of lacustrine sediments (see section "Unit IV/Unit B – Holocene Thermokarst Lake Formation and Lacustrine Sedimentation"). The estimated talik depth based on the core field description following the drilling (3425 cm) was about 2 m deeper than the talik defined by the 0°C boundary based on the borehole temperature measurements (~32 m). This inconsistency is caused by drilling heat that has slightly warmed the sediments in the core, making it challenging to visually identify the frozen-unfrozen boundary in the core during the field description. Temperature data from the lake from 1984 indicated that the talik was about 30 m deep (Grigoriev, 1993), which is similar to our findings.

The homogeneous water contents across all units of the long sediment core, with the exception of the uppermost and lowermost samples, suggest that variations are due to potential changes in pore space. The higher OM content in some samples of the fluvial unit may have led to a higher water content, although Strauss et al. (2012) found that the TOC content was too low to affect the total absolute water content of frozen Yedoma substantially. Nevertheless, higher TOC values can be a reason for the increasing water contents toward the top of the core.

FIGURE 7 | n-Alkane proxies for aquatic (P_{aq}) vs. terrestrial (P_{wax}) plant input of Goltsovoye Lake sediment core PG2412. Unit I: orange stars, Unit II: green circles, Unit III: blue triangles, Unit IV: purple squares.

The electrical conductivity is low (**Figure 4**), reflecting a meteoric source for pore waters in interaction with sediment. The electrical conductivity variations over depth might be explained by variation in solid phase surface area: low in Unit I and high in Unit II, leading to lower concentrations in the thawed Unit I and dissolution of mineral material in Unit II. The upwardly decreasing conductivity in Units III and IV suggests a combination of interactions with the solid phase and diffusive exchange with lake water, which has a conductivity of around 200 μS/cm (Strauss et al., 2018). The EC values in the pore water of the Yedoma sediments (669–1301 μS cm^{-1}, median: 812 μS cm^{-1}) are comparable to thawed Yedoma sediments studied in the Ivashkina Lagoon (Schirrmeister et al., 2018). They found that the EC of water extracts from undisturbed Yedoma sediments at the Mamontovy Khayata were an order of magnitude lower.

Unit I – Early Weichselian Fluvial Sedimentation
The coarser sediments and the presence of rounded pebbles in Unit I and the lower part of Unit II, point to a strong fluvial influence. Significant differences in the biogeochemistry (**Figure 8**) and hydrochemistry between Unit I and II (TOC: $p < 0.05$, δ^{13}C: $p < 0.01$, water content: $p < 0.01$, pH: $p < 0.01$ and EC: $p < 0.01$) corroborates a different source material. Previous studies found fluvial sediments underneath the Yedoma deposits on the Bykovsky Peninsula (Slagoda, 1993; Siegert et al., 2002; Grosse et al., 2007; Schirrmeister et al., 2008b), similar to sites in the Lena Delta (Schirrmeister et al., 2003; Wetterich et al., 2008) and on Cape Mamontov Klyk at the western Laptev Sea coast (Schirrmeister et al., 2008a). On the Bykovsky Peninsula, the meandering paleo-Lena River deposited fluvial sediments during the early Weichselian period (100–50 ka BP) (Kunitsky, 1989; Slagoda, 1993, 2004, 2005; Wetterich et al., 2008). The two infinite ages we found in Unit I at 3662 and 3552 cm and the coarse fluvial material suggest that Unit I underneath Goltsovoye Lake has likely formed as part of a regional fluvial depositional environment of the early Weichselian.

The transport and input of allochthonous organic material (large organic remains and driftwood; **Supplementary Figure 2**) by the paleo-river also explains the high variability and the high values of TOC and n-alkane concentrations (g^{-1} sed.) in Unit I compared to Unit II (**Figures 8A,C**). The CPI and OEP are lowest in Unit I (median: 2.5 and 2.2) and significantly lower than in Unit II ($p < 0.01$ and $p < 0.05$, respectively; **Figures 8E,F**), which reflects the strong OM degradation before and during the transport. The organic-rich woody layers in Unit I most likely did not originate from *in situ* growing trees, but are considered an accumulation of fluvial transported driftwood material from further south.
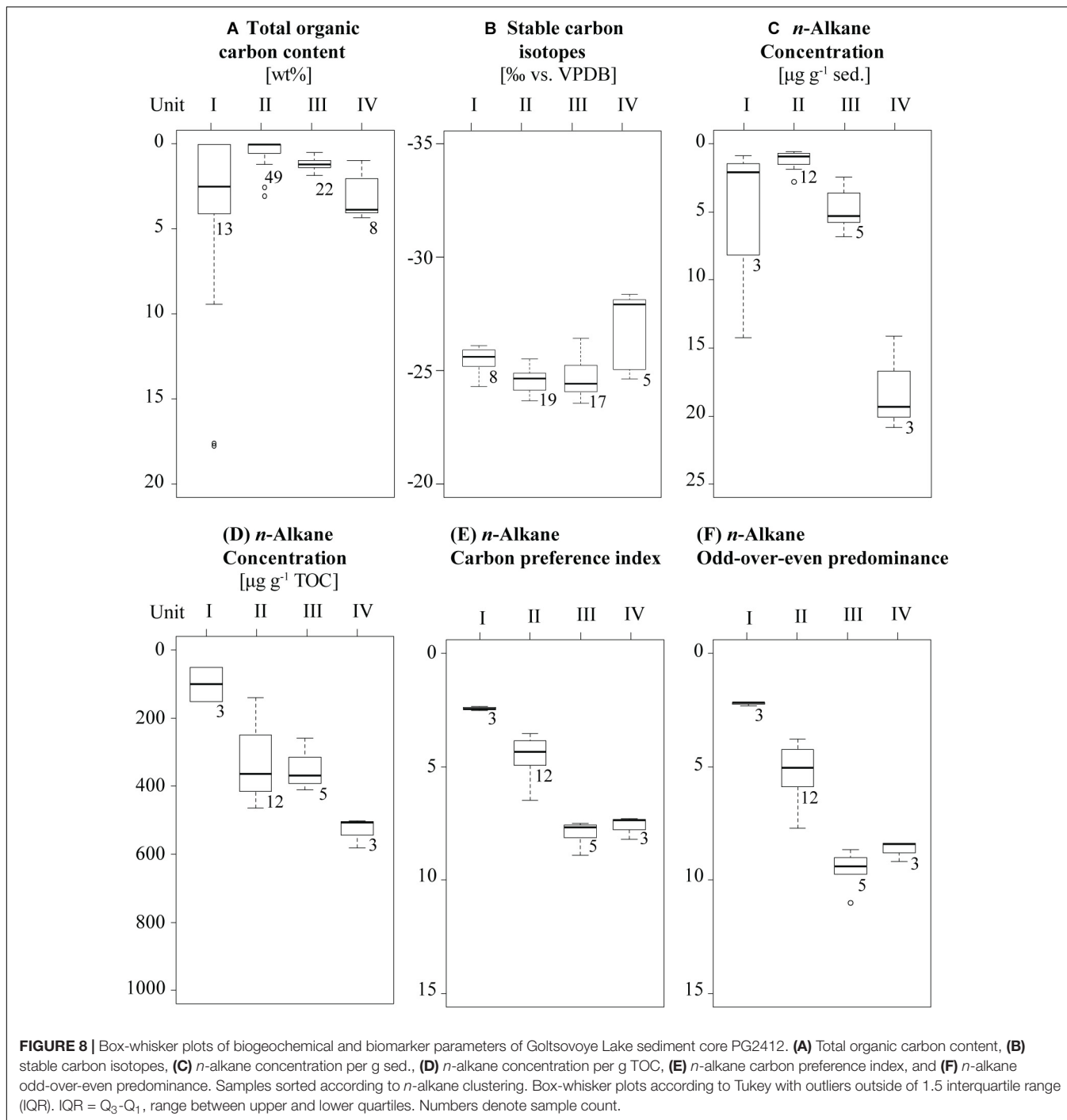
The n-alkane composition is substantially different in Unit I compared to the units above, as can be seen in the proportion of n-C_{23}, n-C_{27} and n-C_{29} and n-C_{31} (**Supplementary Figure 4**). Unit I is enriched in n-C_{23} and has the lowest concentration of n-C_{27} + n-C_{29} and n-C_{31}. The relative abundance of the shorter chains n-C_{23} and n-C_{25} are highest in Unit I (**Figure 6**). Furthermore, the P_{aq}, representing aquatic OM contents, is highest (>0.6) and the P_{wax}, representing terrestrial OM, lowest ($\sim$0.5) (**Figure 7**) in Unit I compared to the other units. Also, the ACL_{23-33}, indicating the main focus of the n-alkane distribution, is lowest ($\sim$26.7) in this unit (**Figure 5C**). The tendency of long chain n-alkanes with lower carbon numbers point to the presence of OM from submerged or floating macrophytes (Ficken et al., 2000), which fits to an aquatic environment in a fluvial regime.

Unit II – Yedoma Deposition in Wetland Landscapes Dominated by Low-Centered Polygons
In the finer, thawed sediments of Unit II (**Supplementary Figure 1**), four of the radiocarbon ages were infinite (**Figure 2A**). Age reversals could point to either reworked sediments or the incorporation of older organic matter. However, in Yedoma sediments, reworking of sediments is not usual due to the syngenetic freezing upon sedimentation. Soil movement as a result of cryoturbation is often restricted to tens of centimeter (Kaiser et al., 2007), while larger cryoturbation patterns sometimes are observed in particular settings. Reworking after *in situ* thawing of the sediments in the talik can happen due to volume loss after melting of ice. Such partial reworking of Yedoma upon thaw underneath lakes was previously described by Farquharson et al. (2016). However, there are no substantial differences in biogeochemical, hydrochemical and n-alkane parameters between samples with finite and infinite ages. Also, the incorporation of allochthonous ancient OM in Yedoma deposits is common (Vasil'chuk and Vasil'chuk, 2017; Jongejans et al., 2018) and hence the most likely explanation of the age reversals in this unit.

The sediments in Unit II are generally OC poor (median TOC: 0.6 wt% and 18 samples with TOC < 0.1 wt%; **Figure 2B**). The low TOC content of the sediments likely results from a combination of OM poor deposition as well as partial OM decomposition after thawing of the sediments. The relatively low CPI and OEP (median: 4.3 and 5.0) reveal partly degraded OM.

The changes in n-alkane distribution (**Supplementary Figure 3**) and relative n-alkane concentration (**Figure 6**) over

FIGURE 8 | Box-whisker plots of biogeochemical and biomarker parameters of Goltsovoye Lake sediment core PG2412. **(A)** Total organic carbon content, **(B)** stable carbon isotopes, **(C)** n-alkane concentration per g sed., **(D)** n-alkane concentration per g TOC, **(E)** n-alkane carbon preference index, and **(F)** n-alkane odd-over-even predominance. Samples sorted according to n-alkane clustering. Box-whisker plots according to Tukey with outliers outside of 1.5 interquartile range (IQR). IQR = Q_3-Q_1, range between upper and lower quartiles. Numbers denote sample count.

depth indicates different OM sources. A lower P_{aq} (0.4–0.5) and higher P_{wax} (0.6–0.7) compared to Unit I (**Figure 7**) and slightly increased ACL_{23-33} values (**Figure 5C**) indicate the presence of emergent macrophytes. The relative large proportion of n-C_{23} and n-C_{25} in Unit I and II (**Figure 6**) is often found in *Sphagnum* mosses (Ficken et al., 1998; Bingham et al., 2010; Bush and McInerney, 2013). The presence of moss points to wet conditions and thus, these findings indicate a wet environment with shallow-water

plant species. Therefore, we interpret this unit as a low-centered polygon environment, whereby water accumulates in the centers of the polygons (Liljedahl et al., 2016). The Yedoma deposition in Unit II could correspond to the relatively wetter conditions of the Kargin Interstadial (Schirrmeister et al., 2002b).

In their study of methane emissions from low-center polygons in the Lena Delta, Kutzbach et al. (2004) found that the amount of methane released relied heavily on the microrelief

of the polygons. Small changes in microrelief led to different hydrologic conditions, thereby influencing the aeration status, OM content and vegetation cover. Also, the water table relative to the roots influences the aeration status. Especially vascular plants can form major pathway for methane transport into the atmosphere. The wetland conditions of the low-centered polygon environment of Unit II probably has led to substantial methane emission in the past.

Unit III/Unit A – Yedoma Deposition Under Cold-Dry Conditions During the Late Weichselian

Unit III of the long sediment core corresponds to Unit A of the short core. Unit III contains one infinite age (at 1559 cm; **Figure 3**) and the dated sample at 1070 cm, which gained a late Pleistocene (MIS 2) age (21.39 ± 0.27 cal ka BP) is older than the general radiocarbon age trend, indicating the presence of reworked or eroded material in this sample. Unit A was deposited during the same period. The age difference between the bulk sediment and the picked plant remains in the short core points to a considerable amount of reworked particulate carbon from the surrounding environment.

The biogeochemical parameters are similar for Units III (median TOC: 1.15 wt%, median δ^{13}C: -24.6‰ vs. VPDB; **Figure 2**) and Unit A (median TOC: 1.7 wt%, median δ^{13}C: -25.0‰ vs. VPDB; **Figure 3**). The multimodal grain size distribution of Unit III (**Supplementary Figure 1**) suggests that multiple transport, accumulation and re-sedimentation processes were involved in the formation, which is in agreement with previous studies of Yedoma deposits (Schirrmeister et al., 2008b; Strauss et al., 2012).

The lower part of Unit III is dominated by n-C_{27} and n-C_{29} and the upper part (at 1158 and 1070 cm) by n-C_{31} suggesting a transition to a grass/herb dominated environment (**Supplementary Figure 3** and **Figure 6**) (Zech et al., 2009; Schäfer et al., 2016). In this interval, also the ACL_{23-33} is shifted to the highest values (**Figure 5C**). The P_{aq} proxy shows the lowest value (below 0.34) and the P_{wax} highest (above 0.75) (**Figure 7**). These findings point to a less aquatic and drier environment, which could correspond to the cold and dry steppe-like tundra that characterized the late Weichselian and the Last Glacial Maximum. This is in agreement with paleo-ecological data from the Mamontovy Khayata Yedoma cliff at the east coast of Bykovsky Peninsula from this period (Schirrmeister et al., 2002b). The TOC and n-alkane concentration (g^{-1} sed.) are significantly higher than in the unit below ($p < 0.01$) (**Figures 8A,C**). The CPI and OEP show maxima at the top of Unit III (median: 7.7 and 9.4; **Figures 8E,F**), indicating that this material shows a low level of degradation.

Few other studies focus on n-alkane concentrations in Siberian Yedoma sediments. The Yedoma sediments from this study (Unit II and III; 138–2455 µg g^{-1} TOC) have n-alkane concentrations comparable to the data from other studied Yedoma deposits in the Ivashkina Lagoon (267–1199 µg g^{-1} TOC) (Ulyantsev et al., 2017), on the Buor Khaya Peninsula (387–1715 µg g^{-1} TOC) (Strauss et al., 2015) and at the cliff of Sobo Sise in the Lena Delta (176–639 µg g^{-1} TOC) (Neubauer, 2016) (**Figure 9A**).
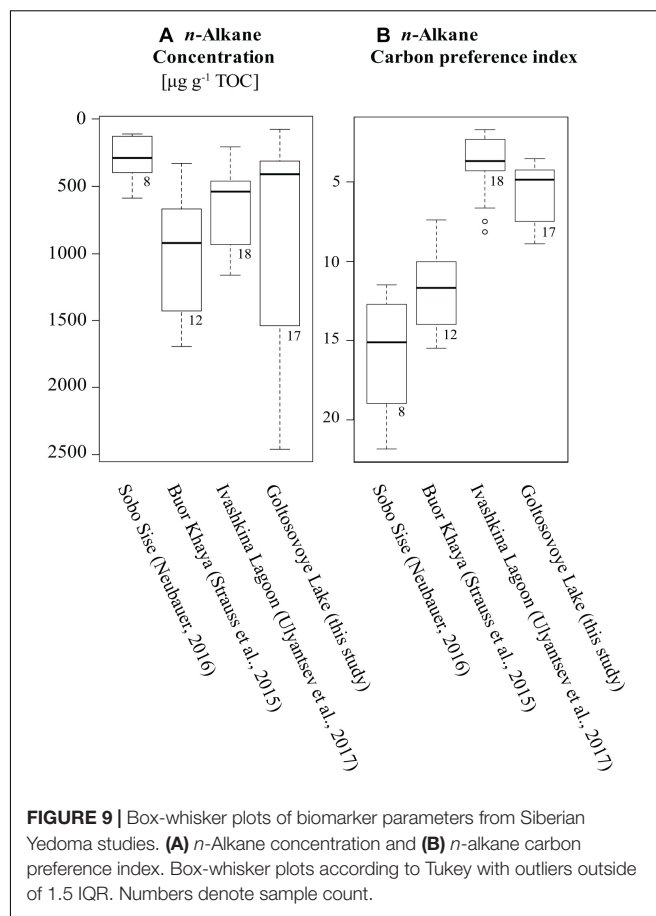

FIGURE 9 | Box-whisker plots of biomarker parameters from Siberian Yedoma studies. **(A)** n-Alkane concentration and **(B)** n-alkane carbon preference index. Box-whisker plots according to Tukey with outliers outside of 1.5 IQR. Numbers denote sample count.

Unit IV/Unit B – Holocene Thermokarst Lake Formation and Lacustrine Sedimentation

Unit IV of the long sediment core corresponds to Unit B of the short core. Unit B1 consists of a peat layer (**Figure 3**). Likely, this basal peaty layer formed during a wetland phase prior to the lake phase and therefore represents the transition to a thermokarst lake. The thickness of the peaty layer of Unit B1 (35 cm) suggests an extended wetland phase. Similar to other young thermokarst lakes (Kessler et al., 2012; Walter Anthony et al., 2018), talik growth and expansion into the previously deposited late Pleistocene Yedoma deposits certainly thawed the Yedoma OM, resulting in high methane production also underneath Goltsovoye Lake. With subsequent lake basin deepening due to subsidence of the thawing ice-rich permafrost, contemporary lake mud containing *in situ* produced OM and reworked old OC from the surrounding slopes accumulated, similarly to other thermokarst lakes in northern Siberia (Biskaborn et al., 2013b; Schleusner et al., 2015).

The radiocarbon age of the peat layer (848 cm depth) is 8 ± 0.05 cal ka BP (**Figure 3**) and probably indicates that thermokarst lake formation started around 8000 years BP. The total thaw depth (talik depth ~32 m, altitude difference between lake and Yedoma uplands ~20 m) of ~52 m is relatively shallow for 8000 years of thermokarst development (M. Angelopoulos, personal communication, 2020). Previous talik modeling studies

of Alaskan thermokarst lakes showed faster talik growth rates for lakes in North America (e.g., Ling and Zhang, 2003; West and Plug, 2008; Kessler et al., 2012; Creighton et al., 2018). However, talik growth could be slowed by characteristics of Siberian Yedoma, such as its higher ice volume in these sediments or the presence of bedfast ice during an extended shallow lake phase (<2 m).

In the long core, the transition from a dry and cold, grass-dominated landscape to a thermokarst lake lies between Unit III and Unit IV. The biogeochemical parameters of Unit IV (median TOC: 3.9 wt%, δ^{13}C: -28.2‰ vs. VPDB; **Figure 2**) are very similar to Unit B (median TOC: 4.2 wt%, median δ^{13}C: -28.6‰ vs. VPDB; **Figure 3**). We found substantial differences between Unit III and IV for the TOC ($p < 0.01$), δ^{13}C ($p < 0.05$) and the n-alkane concentration ($p < 0.05$) (**Figure 8**). Also, the TOC and stable carbon isotope ratio are significantly different between Unit A and B in the short core ($p < 0.01$). The sediments of Unit IV have a higher TOC compared to the thawed Yedoma sediments, which is characteristic for lake sediments with input of lake primary production (Walter Anthony et al., 2014; Jongejans et al., 2018). This is also suggested by the relatively high CPI and OEP in Unit IV (median: 7.3 and 8.4) compared to the lower units.

The dominating n-alkane chain in Unit IV is n-C$_{27}$ (**Supplementary Figure 3**). The ACL, n-alkane ratio, P$_{wax}$, CPI and OEP are lower in Unit IV compared to Unit III (**Figure 8**) and P$_{aq}$ is partly a bit higher. The OM in this unit is likely a mixture derived from primary production in the thermokarst lake and from thawing permafrost surrounding the lake. As found in other thermokarst lake systems, the lake primary productivity is largely influenced by local thermal erosion, surrounding depositional characteristics and drainage processes strongly affecting hydrochemistry and water level (e.g., Biskaborn et al., 2013a; Lenz et al., 2016).
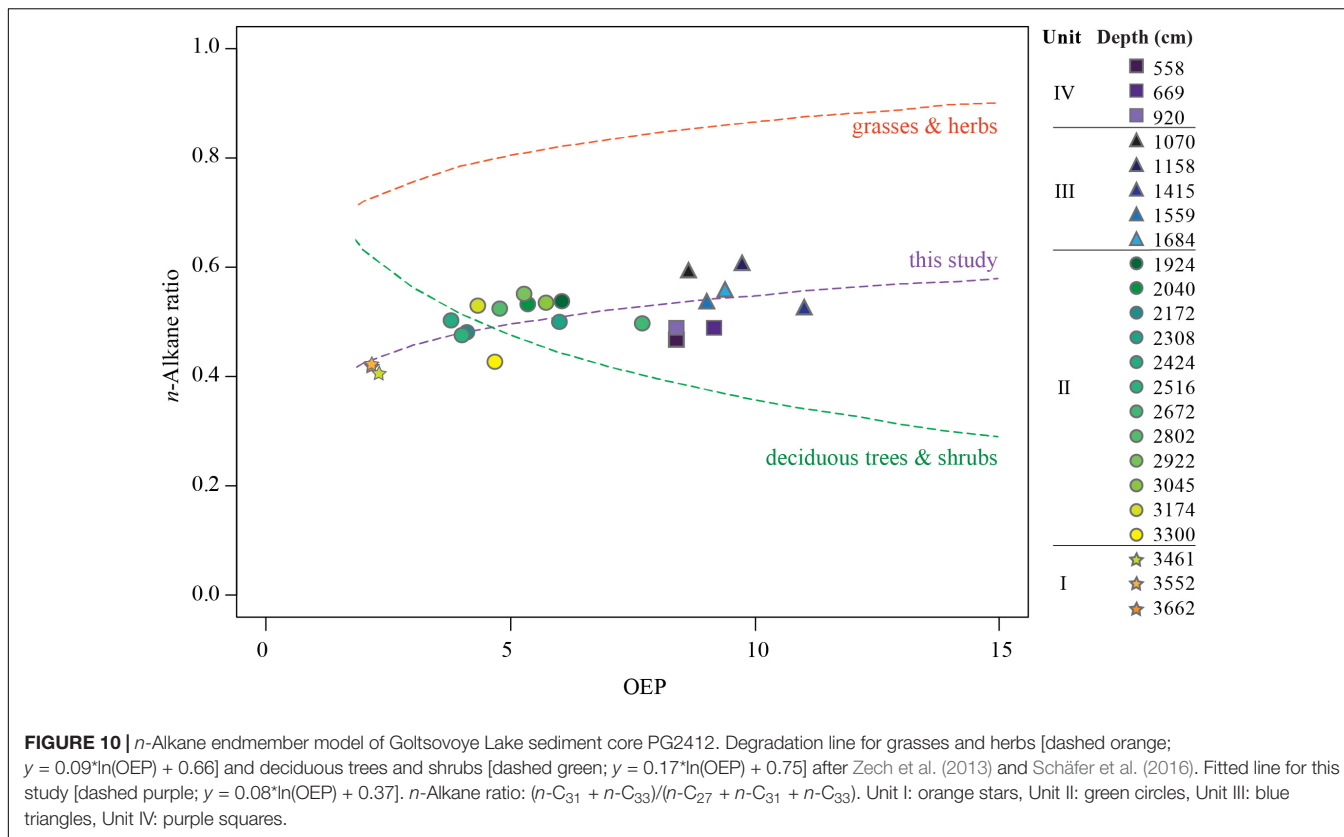
Organic Matter Degradation

The state of OM degradability of Yedoma and other deposits underneath Goltsovoye Lake can be assessed with the n-alkane proxies. In thermokarst-affected Yedoma uplands, the previously undisturbed sediments thaw from the top downwards and therefore, the sediments closer to the surface are expected to have been exposed to thawed conditions for the longest time. Intuitively, one would expect the most degraded OM in the top sediments and the least degraded OM in the bottom sediments of the core. However, based on the CPI and OEP parameters, we found an opposite trend with the furthest degraded OM in the deepest part of the core (**Figures 5D, 8E,F**). As described above, the OM incorporated into the sediments underneath Goltsovoye Lake accumulated under different environmental conditions. Both the OM origin and the depositional conditions have an effect on the CPI and OEP values. Different OM origin and composition lead to different starting values of the parameters for the deposited OM (see for comparison **Figure 9B**) and different environmental conditions can lead to different degradation levels during deposition. Since the OEP and CPI, as well as the n-alkane concentrations and the ACL, show stepwise changes from unit to unit, we interpret the CPI and OEP profiles to be still dominated

by the OM input and the degradation level of the time of deposition was largely preserved, rather than being overprinted by the thaw process underneath the thermokarst lake. Thus, the higher terrestrial character (highest P$_{wax}$) of the OM in Unit III might have caused the highest CPI and OEP values in this core interval, while high degradation of presumably reworked material in the fluvial deposits of Unit I might have led to the lowest values in this core sequence. Overall, the CPI and OEP values still indicate relatively less degraded OM material at least for the Units IV and III and partly also for Unit II.

Romankevich et al. (2017) and Ulyantsev et al. (2017) studied n-alkane parameters of a 38-m-long sediment core from the Ivashkina Lagoon (**Figures 9A,B**), about 3 km east of the Goltsovoye Lake. They found alluvial sands in the bottom (38–22 m), containing highly altered OM (median CPI: 2.7) (Romankevich et al., 2017), which is in line with our findings. In the Yedoma sediments overlying these sands (22–3 m), they distinguished changes in sediment and OM source, as well as burial conditions. In the middle part of the core ($\sim$21–13 m), the OM was enriched in n-C$_{29}$ and n-C$_{31}$, and intermediate bulk CPI values (median: 3.8) could point to microbial degradation. Less-degraded material was found in the upper 5 m of the sediment core. Generally, their interpretation corresponds to our findings. Our n-alkane concentration does not differ significantly in the Ivashkina Yedoma deposits compared to the Goltsovoye Yedoma deposits. However, the OM in the Ivashkina deposits is further degraded (CPI: $p < 0.01$, **Figure 9B**).

We plotted the n-alkane ratio of our samples against the OEP (**Figure 10**). The samples clearly plot according to the n-alkane cluster units with lowest OEP and n-alkane ratio in Unit I and maxima in Unit III. Schäfer et al. (2016) calculated degradation lines for grasses and herbs (orange dashed line) and for deciduous trees and shrubs (green dashed line) based on the data from their study in Central Europe and that of Zech et al. (2013) of eastern Germany. The degradation lines are based on (1) the degradation of the organic material, which is indicated by the OEP, and (2) the vegetation type, which is indicated by the n-alkane ratio. We fitted a logarithmic function to the data of this study (purple dashed line). From this, we argue that the OM in our study contains a mixture of long and mid-chain n-alkanes. Due to the lack of typical deciduous trees and shrubs on the Bykovsky Peninsula, the presence of the n-C$_{27}$ alkanes has to be explained by a different source. Using this endmember model is a first-order approximation to decipher a general pattern. First, one cannot assume a similar plant composition in Arctic regions compared to temperate regions. Second, some plant genera such as *Artemisia* or *Sphagnum*, have been found to have a dominance of the n-C$_{29}$ alkane, thereby 'mimicking' deciduous trees and shrubs (Ficken et al., 1998; Struck et al., 2019). Third, lake aquatic organisms can contribute to mid-chain alkanes (n-C$_{21}$ to n-C$_{27}$), which also leads to the overestimation of the presence of trees and shrubs (Ficken et al., 2000). Finally, samples with poorly preserved OM (low OEP values) can be difficult to interpret, as the degradation signal may have altered the n-alkane patterns (Struck et al., 2018). Even though this endmember model does not seem to reflect the OM source patterns in our samples, it does show a mixed character of the OM. Furthermore, this is

FIGURE 10 | *n*-Alkane endmember model of Goltsovoye Lake sediment core PG2412. Degradation line for grasses and herbs [dashed orange; $y = 0.09*\ln(OEP) + 0.66$] and deciduous trees and shrubs [dashed green; $y = 0.17*\ln(OEP) + 0.75$] after Zech et al. (2013) and Schäfer et al. (2016). Fitted line for this study [dashed purple; $y = 0.08*\ln(OEP) + 0.37$]. *n*-Alkane ratio: $(n\text{-}C_{31} + n\text{-}C_{33})/(n\text{-}C_{27} + n\text{-}C_{31} + n\text{-}C_{33})$. Unit I: orange stars, Unit II: green circles, Unit III: blue triangles, Unit IV: purple squares.

the first time this endmember model has been applied to Arctic sediments samples. More calibrations studies should be carried out to test this promising method for OM characterization studies in Arctic sediments.

In our study, the frozen fluvial sediments below the thawed Yedoma deposits had higher TOC values than in the thawed Yedoma, but this OM at the very bottom of the core also showed a higher level of degradation. The TOC content of the thawed Yedoma deposits is relatively low (median TOC: 0.8 wt% and 22 samples with TOC below detection limit) compared to previous research of still frozen Yedoma on the Bykovsky Peninsula that reported TOC values of 1.2 to 14 wt% (e.g., Schirrmeister et al., 2002a; Strauss et al., 2020). Furthermore, compared to Yedoma deposits on the Buor Khaya Peninsula and the Yedoma cliff of Sobo Sise (median CPI: 11.7 and 15.2, respectively), a degradation signal of the Yedoma OM is traceable (**Figure 9B**). As we have no information about the detailed OM characteristics of undisturbed Yedoma deposits of the study area, we argue that the OM signal of these thawed Yedoma deposits is a mixture of a source signal and a degradation signal of OM thaw and partial microbial decomposition after talik formation. Still, we find that for our biomarker proxies, the OM input signal exceeds the degradation signal in this study.

Continued thermokarst lake growth of Goltsovoye Lake will lead to further talik deepening and thus thawing of more sediments as well as erosion of surrounding sediments into the lake. Walter et al. (2006) showed that methane release at the lake margins accounted for the largest portion of methane

release from thermokarst lakes. As we took our sediment core from the deepest point of the lake, the sediments likely have been thawed the longest time for this lake, while sediments nearer to the shore would have been exposed to thaw only more recently. Our study highlights that thawed deposits underneath a thermokarst lake vary in the OM composition and degradability and that this is primarily a result of OM origin and depositional environment, and less of permafrost thaw history. To understand future responses of further permafrost thaw and to assess the greenhouse gas emission potential, more knowledge is needed about the OM characteristics of the permafrost deposits. A direct comparison of thawed and still frozen Yedoma OM from nearby sites would be useful to better understand the impacts of thaw and microbial decomposition. The applied study of *n*-alkanes proves to be very useful in identifying OM sources, level of degradation and assessment of the depositional environment. Further research using other biogeochemical assessments such as those based on amino acids (Hutchings et al., 2019), *Sphagnum*-derived phenols (Abbott et al., 2013) and pectin-like polysaccharides as well as C/N burial profiles (Schellekens et al., 2015) would also be valuable.

CONCLUSION

Our study of OM degradation in thermokarst-affected permafrost sediments in an ice-rich Yedoma permafrost landscape relied on a unique set of two drilling cores from beneath a thermokarst

lake in northeastern Siberia. Using *n*-alkane indices, we were able to distinguish four depositional units for the frozen and thawed sediments underneath Goltsovoye Lake on Bykovsky Peninsula. The lowest sediments (36.6-33 m) are of fluvial origin and were deposited prior to Yedoma formation. Their OM is characterized by a high degradation level and a relatively large share of aquatic OM (e.g., macrophytes). Yedoma formation started in a relatively wet, low-centered polygon landscape (33-18 m) with low amounts of but largely less degraded OM. Subsequently, *n*-alkane indices indicate a transition to a drier environment during the peak period of the Last Glacial Maximum (18-10 m) that was partly grass dominated (12 to 10 m). Furthermore, the OM in this sediment interval shows a low level of degradation. In the middle Holocene, a thermokarst lake formed and deposited lacustrine sediments (10-5.1 m), accompanied by talik formation that subsequently thawed the previously accumulated ice-rich Yedoma deposits. These lake sediments exhibit a higher TOC and *n*-alkane concentrations compared to the Yedoma sediments below.

Both the Yedoma deposits and the fluvial deposits contain old allochthonous OM. Moreover, using the *n*-alkane endmember model, we found a mixed input of the OM in all units. In the thawed Yedoma sediments, less OC was found compared to frozen Yedoma deposits reported elsewhere, suggesting a combination of OC poor deposition and partial mobilization of OC and release as methane from the thermokarst lake talik. Higher OC contents were found in the frozen fluvial sediments below the Yedoma deposits. However, using the *n*-alkane parameters, we found a trend toward increasingly degraded OM in these sediments in the bottom of the core. Overall, the *n*-alkane proxies suggest that the input signal of the OM still exceeds the degradation signal from thaw underneath the lake and that these parameters can still provide valuable information on the origin, degradation level and deposition conditions of the deposited OM.

DATA AVAILABILITY STATEMENT

All datasets generated for this study are available on PANGAEA.

AUTHOR CONTRIBUTIONS

JS, GG, and MG developed the overall coring plans for the Bykovsky Peninsula field campaign. JS, MG, GM, LS, BB, and GG conducted the field work. LJ and JS developed the study design for biomarker analysis of the core. LJ and BB performed the laboratory analyses and led the data interpretation for the long (PG2412) and short (PG2420) sediment cores, respectively. All co-authors contributed with their specific expertise to data interpretation and provided feedback to the manuscript. LJ led the writing of the manuscript.

FUNDING

ACKNOWLEDGMENTS

SUPPLEMENTARY MATERIAL

The Supplementary Material for this article can be found online at: https://www.frontiersin.org/articles/10.3389/fenvs.2020.00118/full#supplementary-material

REFERENCES

Abbott, G. D., Swain, E. Y., Muhammad, A. B., Allton, K., Belyea, L. R., Laing, C. G., et al. (2013). Effect of water-table fluctuations on the degradation of *Sphagnum* phenols in surficial peats. *Geochim. Cosmochim. Acta* 106, 177–191. doi: 10.1016/j.gca.2012.12.013

Andersson, R. A., and Meyers, P. A. (2012). Effect of climate change on delivery and degradation of lipid biomarkers in a Holocene peat sequence in the Eastern European Russian Arctic. *Org. Geochem.* 53, 63–72. doi: 10.1016/j.orggeochem.2012.05.002

Bingham, E. M., McClymont, E. L., Väliranta, M., Mauquoy, D., Roberts, Z., Chambers, F. M., et al. (2010). Conservative composition of *n*-alkane biomarkers in *Sphagnum* species: implications for palaeoclimate reconstruction in ombrotrophic peat bogs. *Org. Geochem.* 41, 214–220. doi: 10.1016/j.orggeochem.2009.06.010

Biskaborn, B. K., Herzschuh, U., Bolshiyanov, D., Savelieva, L., Zibulski, R., and Diekmann, B. (2013a). Late Holocene thermokarst variability inferred from diatoms in a lake sediment record from the Lena Delta, Siberian Arctic. *J. Paleolimnol.* 49, 155–170. doi: 10.1007/s10933-012-9650-1

Biskaborn, B. K., Herzschuh, U., Bolshiyanov, D. Y., Schwamborn, G., and Diekmann, B. (2013b). Thermokarst processes and depositional events in a tundra lake, northeastern Siberia. *Permafr. Periglac. Process.* 24, 160–174. doi: 10.1002/ppp.1769

Biskaborn, B. K., and Sens, M. (2020). *Biogeochemical And Radiocarbon Data Of Sediment Core PG2420*. Bykovsky Peninsula: Great Lake Publishing.

Biskaborn, B. K., Smith, S. L., Noetzli, J., Matthes, H., Vieira, G., Streletskiy, D. A., et al. (2019). Permafrost is warming at a global scale. *Nat. Commun.* 10:264. doi: 10.1038/s41467-018-08240-4

Bray, E. E., and Evans, E. D. (1961). Distribution of *n*-paraffins as a clue to recognition of source beds. *Geochim. Cosmochim. Acta* 22, 2–15. doi: 10.1016/0016-7037(61)90069-2

Bush, R. T., and McInerney, F. A. (2013). Leaf wax *n*-alkane distributions in and across modern plants: implications for paleoecology and chemotaxonomy. *Geochim. Cosmochim. Acta* 117, 161–179. doi: 10.1016/j.gca.2013.04.016

Creighton, A. L.-T., Parsekian, A. D., Angelopoulos, M., Jones, B. M., Bondurant, A. C., Engram, M., et al. (2018). Transient electromagnetic surveys for the determination of talik depth and geometry beneath thermokarst lakes. *J. Geophys. Res. Solid Earth* 123, 9310–9323. doi: 10.1029/2018JB016121

Farquharson, L., Anthony, K. W., Bigelow, N., Edwards, M., and Grosse, G. (2016). Facies analysis of yedoma thermokarst lakes on the northern Seward Peninsula, Alaska. *Sediment. Geol.* 340, 25–37. doi: 10.1016/j.sedgeo.2016.01.002

Ficken, K. J., Barber, K. E., and Eglinton, G. (1998). Lipid biomarker, δ13C and plant macrofossil stratigraphy of a Scottish montane peat bog over the last two millennia. *Org. Geochem.* 28, 217–237. doi: 10.1016/S0146-6380(97)00126-125

Ficken, K. J., Li, B., Swain, D., and Eglinton, G. (2000). An *n*-alkane proxy for the sedimentary input of submerged/floating freshwater aquatic macrophytes. *Org. Geochem.* 31, 745–749. doi: 10.1016/S0146-6380(00)00081-4

French, H. M. (1999). Past and present permafrost as an indicator of climate change. *Polar Res.* 18, 269–274. doi: 10.3402/polar.v18i2.6584

Fuchs, M., Grosse, G., Strauss, J., Günther, F., Grigoriev, M., Maximov, G. M., et al. (2018). Carbon and nitrogen pools in thermokarst-affected permafrost landscapes in Arctic Siberia. *Biogeosciences* 15, 953–971. doi: 10.5194/bg-15-953-2018

Gaglioti, B. V., Mann, D. H., Jones, B. M., Pohlman, J. W., Kunz, M. L., and Wooller, M. J. (2014). Radiocarbon age-offsets in an arctic lake reveal the long-term response of permafrost carbon to climate change. *J. Geophys. Res. Biogeosciences* 119, 1630–1651. doi: 10.1002/2014JG002688

Grigoriev, M. (1993). *Cryomorphogenesis of the Lena River Mouth Area.* Novosibirsk: Siberian Branch.

Grigoriev, N. (1960). The temperature of permafrost in the Lena delta basin-deposit conditions and properties of the permafrost in Yakutia. *Yakutsk* 2, 97–101.

Grosse, G., Schirrmeister, L., Kunitsky, V., Rachold, V., Grigoriev, M. N., and Hubberten, H.-W. (2005). "Volumetric balance of ice complex deposits at Bykovsky Peninsula (NE Siberia), using field data, remote sensing and digital elevation models," in *Proceedings of the 2nd European Conference on Permafrost*, Potsdam.

Grosse, G., Schirrmeister, L., Siegert, C., Kunitsky, V. V., Slagoda, E. A., Andreev, A. A., et al. (2007). Geological and geomorphological evolution of a sedimentary periglacial landscape in Northeast Siberia during the late quaternary. *Geomorphology* 86, 25–51. doi: 10.1016/j.geomorph.2006.08.005

Heslop, J. K., Anthony, K. M. W., Grosse, G., Liebner, S., and Winkel, M. (2019). Century-scale time since permafrost thaw affects temperature sensitivity of net methane production in thermokarst-lake and talik sediments. *Sci. Total Environ.* 691, 124–134. doi: 10.1016/j.scitotenv.2019.06.402

Höfle, S., Rethemeyer, J., Mueller, C. W., and John, S. (2013). Organic matter composition and stabilization in a polygonal tundra soil of the Lena Delta. *Biogeosciences* 10, 3145–3158. doi: 10.5194/bg-10-3145-2013

Hugelius, G., Strauss, J., Zubrzycki, S., Harden, J. W., Schuur, E. A. G., Ping, C.-L., et al. (2014). Estimated stocks of circumpolar permafrost carbon with quantified uncertainty ranges and identified data gaps. *Biogeosciences* 11, 6573–6593. doi: 10.5194/bg-11-6573-2014

Hutchings, J. A., Bianchi, T. S., Kaufman, D. S., Kholodov, A. L., Vaughn, D. R., and Schuur, E. A. G. (2019). Millennial-scale carbon accumulation and molecular transformation in a permafrost core from Interior Alaska. *Geochim. Cosmochim. Acta* 253, 231–248. doi: 10.1016/j.gca.2019.03.028

Jenrich, M. (2020). *Thermokarst Lagoons - Carbon Pools and Panarctic Distribution.* Master thesis, University of Potsdam, Potsdam.

Jongejans, L. L., Mangelsdorf, K., and Strauss, J. (2020). n-Alkanes, total organic carbon content, radiocarbon ages, grain size distribution, biogeochemical and hydrochemical parameters of sediment core beneath thermokarst lake

Goltsovoye Lake on the Bykovsky Pensinula, northeastern Siberia. *PANGAEA.* doi: 10.1594/PANGAEA.919811

Jongejans, L. L., Strauss, J., Lenz, J., Peterse, F., Mangelsdorf, K., Fuchs, M., et al. (2018). Organic matter characteristics in yedoma and thermokarst deposits on Baldwin Peninsula, west Alaska. *Biogeosciences* 15, 6033–6048. doi: 10.5194/bg-15-6033-2018

Kaiser, C., Meyer, H., Biasi, C., Rusalimova, O., Barsukov, P., and Richter, A. (2007). Conservation of soil organic matter through cryoturbation in arctic soils in Siberia. *J. Geophys. Res. Biogeosciences* 112:258. doi: 10.1029/2006JG000258

Kessler, M. A., Plug, L. J., and Walter Anthony, K. M. (2012). Simulating the decadal- to millennial-scale dynamics of morphology and sequestered carbon mobilization of two thermokarst lakes in NW Alaska. *J. Geophys. Res. Biogeosciences* 117:1796. doi: 10.1029/2011JG001796

Killops, S. D., and Killops, V. J. (2013). "5.1.2 General differences between major groups of organisms," in *Introduction to Organic Geochemistry*, (Somerset: Wiley), 167.

Knoblauch, C., Beer, C., Sosnin, A., Wagner, D., and Pfeiffer, E.-M. (2013). Predicting long-term carbon mineralization and trace gas production from thawing permafrost of Northeast Siberia. *Glob. Change Biol.* 19, 1160–1172. doi: 10.1111/gcb.12116

Kunitsky, V. V. (1989). *Kriolitologiya Nizo'ev Leny (Cryolithology ofthe Lower LENA).* Yakutsk: Permafrost Institute Press.

Kutzbach, L., Wagner, D., and Pfeiffer, E.-M. (2004). Effect of microrelief and vegetation on methane emission from wet polygonal tundra, Lena Delta, Northern Siberia. *Biogeochemistry* 69, 341–362. doi: 10.1023/B:BIOG.0000031053.81520.db

Lacelle, D., Fontaine, M., Pellerin, A., Kokelj, S. V., and Clark, I. D. (2019). Legacy of holocene landscape changes on soil biogeochemistry: a perspective from paleo-active layers in Northwestern Canada. *J. Geophys. Res. Biogeosci.* 124, 2662–2679. doi: 10.1029/2018JG004916

Lenz, J., Jones, B. M., Wetterich, S., Tjallingii, R., Fritz, M., Arp, C. D., et al. (2016). Impacts of shore expansion and catchment characteristics on lacustrine thermokarst records in permafrost lowlands. Alaska Arctic Coastal Plain. *Arktos* 2:25. doi: 10.1007/s41063-016-0025-0

Liljedahl, A. K., Boike, J., Daanen, R. P., Fedorov, A. N., Frost, G. V., Grosse, G., et al. (2016). Pan-Arctic ice-wedge degradation in warming permafrost and its influence on tundra hydrology. *Nat. Geosci.* 9, 312–318. doi: 10.1038/ngeo2674

Ling, F., and Zhang, T. (2003). Numerical simulation of permafrost thermal regime and talik development under shallow thaw lakes on the Alaskan Arctic Coastal Plain. *J. Geophys. Res. Atmos.* 108:3014. doi: 10.1029/2002JD003014

Mackelprang, R., Waldrop, M. P., DeAngelis, K. M., David, M. M., Chavarria, K. L., Blazewicz, S. J., et al. (2011). Metagenomic analysis of a permafrost microbial community reveals a rapid response to thaw. *Nature* 480, 368–371. doi: 10.1038/nature10576

Marzi, R., Torkelson, B. E., and Olson, R. K. (1993). A revised carbon preference index. *Org. Geochem.* 20, 1303–1306. doi: 10.1016/0146-6380(93)90016-5

Neubauer, D. (2016). *Characterization Of Organic Matter Stored In Yedoma And Thermokarst Permafrost.* Master thesis, Freie Universität, Berlin.

Poynter, J., and Eglinton, G. (1990). "14. Molecular composition of three sediments from hole 717c: the Bengal fan," in *Proceedings of the Ocean Drilling Program: Scientific Results*, College Station, TX.

Radke, M., Willsch, H., and Welte, D. H. (1980). Preparative hydrocarbon group type determination by automated medium pressure liquid chromatography. *Anal. Chem.* 52, 406–411. doi: 10.1021/ac50053a009

Romankevich, E. A., Vetrov, A. A., Belyaev, N. A., Sergienko, V. I., Semiletov, I. P., Sukhoverkhov, S. V., et al. (2017). Alkanes in quaternary deposits of the Laptev Sea. *Dokl. Earth Sci.* 472, 36–39. doi: 10.1134/S1028334X17010093

Romanovskii, N. (1993). *Fundamentals of Cryogenesis Of Lithosphere.* Moscow: Moscow University Press.

Sánchez-García, L., Vonk, J. E., Charkin, A. N., Kosmach, D., Dudarev, O. V., Semiletov, I. P., et al. (2014). Characterisation of three regimes of collapsing arctic ice complex deposits on the SE laptev sea coast using biomarkers and dual carbon isotopes. *Permafr. Periglac. Process.* 25, 172–183. doi: 10.1002/ppp.1815

Schäfer, I. K., Lanny, V., Franke, J., Eglinton, T. I., Zech, M., Vysloužilová, B., et al. (2016). Leaf waxes in litter and topsoils along a european transect. *Soil* 2, 551–564. doi: 10.5194/soil-2-551-2016

Schellekens, J., Bindler, R., Martínez-Cortizas, A., McClymont, E. L., Abbott, G. D., Biester, H., et al. (2015). Preferential degradation of polyphenols in *Sphagnum* - 4-Isopropenylphenol as a proxy for past hydrological conditions in *Sphagnum*-dominated peat. *Geochim. Cosmochim. Acta* 150, 74–89. doi: 10. 1016/j.gca.2014.12.003

Schirrmeister, L., Froese, D., Tumskoy, V., Grosse, G., and Wetterich, S. (2013). "Yedoma: late pleistocene ice-rich syngenetic permafrost of Beringia," in *Encyclopedia of Quaternary Science*, eds S. A. Elias, C. J. Mock, and J. Murton (Amsterdam: Elsevier), doi: 10.1016/B978-0-444-53643-3.00106-0

Schirrmeister, L., Grigoriev, M. N., Strauss, J., Grosse, G., Overduin, P. P., Kholodov, A., et al. (2018). Sediment characteristics of a thermokarst lagoon in the northeastern Siberian Arctic (Ivashkina Lagoon, Bykovsky Peninsula). *Arktos* 4:13. doi: 10.1007/s41063-018-0049-8

Schirrmeister, L., Grosse, G., Kunitsky, V., Magens, D., Meyer, H., Dereviagin, A., et al. (2008a). Periglacial landscape evolution and environmental changes of Arctic lowland areas for the last 60 000 years (western Laptev Sea coast, Cape Mamontov Klyk). *Polar Res.* 27, 249–272. doi: 10.1111/j.1751-8369.2008. 00067.x

Schirrmeister, L., Kunitsky, V. V., Grosse, G., Kuznetsova, T. V., Derevyagin, A. Y., Wetterich, S., et al. (2008b). "The yedoma suite of the Northeastern Siberian shelf region characteristics and concept of formation," in *Proceedings of the Ninth International Conference on Permafrost*, Fairbanks.

Schirrmeister, L., Grosse, G., Schwamborn, G., Andreev, A., Meyer, H., Kunitsky, V. V., et al. (2003). Late Quaternary history of the accumulation plain north of the chekanovsky ridge (Lena Delta, Russia) - a multidisciplinary approach. *Polar Geogr.* 27, 277–319. doi: 10.1080/789610225

Schirrmeister, L., Siegert, C., Kunitzky, V. V., Grootes, P. M., and Erlenkeuser, H. (2002a). Late quaternary ice-rich permafrost sequences as a paleoenvironmental archive for the Laptev Sea region in northern Siberia. *Int. J. Earth Sci.* 91, 154–167. doi: 10.1007/s005310100205

Schirrmeister, L., Siegert, C., Kuznetsova, T., Kuzmina, S., Andreev, A., Kienast, F., et al. (2002b). Paleoenvironmental and paleoclimatic records from permafrost deposits in the Arctic region of Northern Siberia. *Quat. Int.* 89, 97–118. doi: 10.1016/S1040-6182(01)00083-0

Schleusner, P., Biskaborn, B. K., Kienast, F., Wolter, J., Subetto, D., and Diekmann, B. (2015). Basin evolution and palaeoenvironmental variability of the thermokarst lake E l'gene-K yuele, Arctic Siberia. *Boreas* 44, 216–229. doi: 10.1111/bor.12084

Schulte, S., Mangelsdorf, K., and Rullkötter, J. (2000). Organic matter preservation on the Pakistan continental margin as revealed by biomarker geochemistry. *Org. Geochem.* 31, 1005–1022. doi: 10.1016/S0146-6380(00)00108-X

Schuur, E. A. G., McGuire, A. D., Schädel, C., Grosse, G., Harden, J. W., Hayes, D. J., et al. (2015). Climate change and the permafrost carbon feedback. *Nature* 520:171. doi: 10.1038/nature14338

Siegert, C., Schirrmeister, L., and Babiy, O. (2002). The sedimentological, mine-ralogical and geochemical composition of late Pleistocene deposits from the ice complex on the Bykovsky peninsula, northern Siberia. *Polarforsch.* 70, 3–11.

Slagoda, E. A. (1993). *Genesis i Mikrostroenie Kriolitogennykh Otlozhenii Bykovskogo Polyostrova i Ostrova Muoastakh [Genesis and Microstructure Of Cryolithogenic Deposits At The Bykovsky Peninsula and the Muostakh Island].* Ph.D. thesis, Permafrost Institute Yakutsk, Yakutsk.

Slagoda, E. A. (2004). *Kriogennye Otlozheniya Primorskoi Ravninymorya Laptebykh: Litologiya I Mikromorfologiya [CryolithogenicDeposits of the Laptev Sea Coastal Plain: Lithology and Micromorphology].* Tyumen: Express Printing Center.

Slagoda, E. A. (2005). "Cryogenic structure and genesis of late cenozoicwatershed formations at the primorsky mountain range adjacent to the Bykovsky Peninsula, Laptev Sea, Russia," in *2nd European Conference on Permafrost*, Potsdam, Germany, 23–24.

Stapel, J. G., Schwamborn, G., Schirrmeister, L., Horsfield, B., and Mangelsdorf, K. (2018). Substrate potential of last interglacial to holocene permafrost organic matter for future microbial greenhouse gas production. *Biogeosciences* 15, 1969–1985. doi: 10.5194/bg-15-1969-2018

Strauss, J., Boike, J., Bolshiyanov, D. Y., Grigoriev, M. N., El-Hajj, H., Morgenstern, A., et al. (2018). *Russian-German Cooperation: Expeditions to Siberia in 2017.* Bremerhaven: Alfred Wegener Institute for Polar and Marine Research.

Strauss, J., Laboor, S., Schirrmeister, L., Grosse, G., Fortier, D., Hugelius, G., et al. (2020). *Yedoma and Thermokarst Site Characteristics From Sample Analysis,*

1998-2016, Alaska (US), Northern Siberia (RU). Bremerhaven: Alfred Wegener Institute for Polar and Marine Research.

Strauss, J., Schirrmeister, L., Grosse, G., Fortier, D., Hugelius, G., Knoblauch, C., et al. (2017). Deep Yedoma permafrost: a synthesis of depositional characteristics and carbon vulnerability. *Earth Sci. Rev.* 172, 75–86. doi: 10. 1016/j.earscirev.2017.07.007

Strauss, J., Schirrmeister, L., Grosse, G., Wetterich, S., Ulrich, M., Herzschuh, U., et al. (2013). The deep permafrost carbon pool of the yedoma region in Siberia and Alaska. *Geophys. Res. Lett.* 40, 6165–6170. doi: 10.1002/2013GL05 8088

Strauss, J., Schirrmeister, L., Mangelsdorf, K., Eichhorn, L., Wetterich, S., and Herzschuh, U. (2015). Organic-matter quality of deep permafrost carbon - a study from Arctic Siberia. *Biogeosciences* 12, 2227–2245. doi: 10.5194/bg-12-2227-2015

Strauss, J., Schirrmeister, L., Wetterich, S., Borchers, A., and Davydov, S. P. (2012). Grain-size properties and organic-carbon stock of Yedoma ice complex permafrost from the Kolyma lowland, northeastern Siberia. *Glob. Biogeochem. Cycles* 26:2011GB004104. doi: 10.1029/2011GB004104

Struck, J., Bliedtner, M., Strobel, P., Schumacher, J., Bazarradnaa, E., and Zech, R. (2019). Leaf wax *n*-alkane pattern and compound-specific δ13C of plants and topsoils from semi-arid Mongolia. *Biogeosciences Discuss.* 2019, 1–23. doi: 10.5194/bg-2019-251

Struck, J., Roettig, C. B., Faust, D., and Zech, R. (2018). Leaf waxes from aeolianite-paleosol sequences on Fuerteventura and their potential for paleoenvironmental and climate reconstructions in the arid subtropics. *EG Quat. Sci. J.* 66, 109–114. doi: 10.5194/egqsj-66-109-2018

Stuiver, M., Reimer, P. J., and Reimer, R. W. (2017). *CALIB 14C Calibration Program*. Available online at: http://calib.org/calib/ (accessed December 13, 2017).

Treshnikov, A. (1985). *Atlas Arktiki [Atlas of the Arctic]*. Available online at: https: //www.worldcat.org/title/atlas-arktiki/oclc/14694389 (accessed February 15, 2020).

Turetsky, M. R., Abbott, B. W., Jones, M. C., Anthony, K. W., Olefeldt, D., Schuur, E. A. G., et al. (2020). Carbon release through abrupt permafrost thaw. *Nat. Geosci.* 13, 138–143. doi: 10.1038/s41561-019-0526-0

Ulyantsev, A. S., Romankevich, E. A., Bratskaya, S. Yu, Prokuda, N. A., Sukhoverkhov, S. V., Semiletov, I. P., et al. (2017). Characteristic of quaternary sedimentation on a shelf of the Laptev Sea according to the molecular composition of *n*-alkanes. *Dokl. Earth Sci.* 473, 449–453. doi: 10.1134/ S1028334X17040158

Vasil'chuk, Y. K., and Vasil'chuk, A. C. (2017). Validity of radiocarbon ages of *Siberian yedoma. Geol. Res. J.* 13, 83–95. doi: 10.1016/j.grj.2017.02.004

Walter, K. M., Zimov, S. A., Chanton, J. P., Verbyla, D., and Chapin, F. S. (2006). Methane bubbling from Siberian thaw lakes as a positive feedback to climate warming. *Nature* 443, 71–75. doi: 10.1038/nature05040

Walter Anthony, K., Schneider von Deimling, T., Nitze, I., Frolking, S., Emond, A., Daanen, R., et al. (2018). 21st-century modeled permafrost carbon emissions accelerated by abrupt thaw beneath lakes. *Nat. Commun.* 9:3262. doi: 10.1038/ s41467-018-05738-9

Walter Anthony, K. M., Zimov, S. A., Grosse, G., Jones, M. C., Anthony, P. M. III, Chapin, F. S., et al. (2014). A shift of thermokarst lakes from carbon sources to sinks during the holocene epoch. *Nature* 511, 452–456. doi: 10.1038/ nature13560

West, J. J., and Plug, L. J. (2008). Time-dependent morphology of thaw lakes and taliks in deep and shallow ground ice. *J. Geophys. Res. Earth Surf.* 113:697. doi: 10.1029/2006JF000696

Wetterich, S., Kuzmina, S., Andreev, A. A., Kienast, F., Meyer, H., Schirrmeister, L., et al. (2008). Palaeoenvironmental dynamics inferred from late quaternary permafrost deposits on Kurungnakh Island, Lena Delta, Northeast Siberia, Russia. *Quat. Sci. Rev.* 27, 1523–1540. doi: 10.1016/j.quascirev.2008. 04.007

Wetterich, S., Schirrmeister, L., Andreev, A., Pudenz, M., Plessen, B., Meyer, H., et al. (2009). Eemian and Late Glacial/holocene palaeoenvironmental records from permafrost sequences at the dmitry laptev strait (NE Siberia, Russia). *Palaeogeogr. Palaeoclimatol. Palaeoecol.* 279, 73–95. doi: 10.1016/j.palaeo.2009. 05.002

Zech, M., Andreev, A., Zech, R., Müller, S., Hambach, U., Frechen, M., et al. (2010). Quaternary vegetation changes derived from a loess-like permafrost palaeosol

sequence in northeast Siberia using alkane biomarker and pollen analyses. *Boreas* 393, 540–550. doi: 10.1111/j.1502-3885.2009.00132.x

Zech, M., Buggle, B., Leiber, K., Marković, S., Glaser, B., Hambach, U., et al. (2009). Reconstructing Quaternary vegetation history in the Carpathian Basin, SE-Europe, using *n*-alkane biomarkers as molecular fossils: problems and possible solutions, potential and limitations. *EG Quat. Sci. J.* 58, 148–155. doi: 10.3285/eg.58.2.03

Zech, M., Krause, T., Meszner, S., and Faust, D. (2013). Incorrect when uncorrected: reconstructing vegetation history using *n*-alkane biomarkers in loess-paleosol sequences - a case study from the saxonian loess region, Germany. *Quat. Int.* 296, 108–116. doi: 10.1016/j.quaint.2012.01.023

Zheng, Y., Zhou, W., Meyers, P. A., and Xie, S. (2007). Lipid biomarkers in the Zoigê-Hongyuan peat deposit: indicators of holocene climate changes in West China. *Org. Geochem.* 38, 1927–1940. doi: 10.1016/j.orggeochem.2007.06.012

Zimov, S. A., Voropaev, Y. V., Semiletov, I. P., Davidov, S. P., Prosiannikov, S. F., Chapin, F. S., et al. (1997). North siberian lakes: a methane source fueled by pleistocene carbon. *Science* 277, 800–802. doi: 10.1126/science.277.5327.800